Aalen University

Faculty of Optometry

Validation of a measuring device constructed on bases of the principle of the center of rotation of the eye.

Bachelor's Thesis

by Benjamin Hahn

Supervisor:	Prof. Dr. Ulrike Paffrath
Second Supervisor:	Reinhard Liebhäußer
Submission Date:	04.08.2014

Abstract

Ophthalmic lenses are ideally measured in accordance with the center of rotation of the eye. Therefore a measuring device was constructed due to this principle to measure lenses with a focimeter. In this work that measuring device was validated. Lenses of ±4 dpt in spherical and aspherical design were measured across a field of 9x9 measuring points being at 5° distance from each other. This corresponds to a field of view of 40°. The measurement points in x- and y-direction were theoretically calculated to validate the measurement results. Regarding angles of incidence up to 20° it was supposed that the main optical aberration depends on a change in the sagittal and tangential sphere powers which is also defined as astigmatism. Therefore the calculation presents the tangential and sagittal oblique sphere powers depending on the different angles of the line of vision.

On average the measurement results and the calculated data of the spherical designed lenses coincide quite good (correlation at 0,98), the systematic deviation of both values on average is 0.01 dpt and the random error (standard deviation) amounts 0.03 dpt on average. The minimum deviation is -0.06 dpt and the maximum is 0.09 dpt. Common focimeters have a measuring inaccuracy of up to 0.06 dpt (Diepes, Blendowske 2002). Therefore the quality of the measured data should be reliable.

The aspherical designed lenses were compared to the spherical designed lenses. With increased angles of incidence the astigmatism of the aspherical lenses leads to lower values than the astigmatism of the spherical lenses.

Content

Declaration of Authorship

I hereby certify that this thesis has been composed by me and is based on my own work, unless stated otherwise. No other person's work has been used without due acknowledgement in this thesis. All references and verbatim extracts have been quoted, and all sources of information, including graphs and data sets, have been specifically acknowledged.

Date Signature

Acknowledgment

I would like to express my gratitude to my supervisor, Prof. Dr. Ulrike Paffrath, whose expertise, understanding, and patience, added considerably to my graduate experience. And of course I want to thank her for providing the topic of this thesis. I also would like to thank the second supervisor, Reinhard Liebhäußer for the assistance in the process of measuring and for constructing and creating the measuring device which is subject of this thesis.

I would also like to thank my whole family for the support they provided me through my entire life and especially through my duration of study. I want to thank my parents that they gave me the opportunity to study. A very special gratitude goes to my wife Sara who helped me with her understanding love and encouragement to finish this thesis.

1 Introduction

The gaze of a latent eye hits the center of a spectacle lens. De facto no eye is latent, but there is movement of the eye. In the process of the eye's movement the glasses are not moved. Therefore dependent on the angle of gaze one looks through different parts of an ophthalmic lens. The eye itself rotates about the so-called center of rotation of the eye Z'. This is the operating situation of a normal ophthalmic lens. Therefore it is of interest to measure an ophthalmic lens in accordance to this principle of the eye's center of rotation.

Aalen University's laboratory supervisor in optometry, Reinhard Liebhäußer, has constructed a rotatable measuring device to simulate this principle. The aim of this thesis is the validation of that measuring device.

First, one has to consider the optical aberrations which might occur at any ophthalmic lens. It is important to elaborate which optical aberrations have the strongest impact on the imaging quality due to increasing angles of the viewing direction. Those aberrations then have to be calculated and compared to the measured results for a specific lens. The comparison of the measured results and the calculated values serves to validate the measuring device.

2 Theoretical Foundations

2.1 Focimeter

In ophthalmic optics, spectacles are specified in terms of their back vertex power, front surface power and refractive index and thickness, instead of their equivalent power. Thus the measurement of vertex powers is the most common power measurement in ophthalmic optics, and furthermore it is simpler to measure the vertex power than to measure equivalent power. A simple instrument for measuring vertex powers is the focimeter. (Smith, Atchison 1997)

The applied method is equally suitable for negative as well as positive vertex power lenses. In figure 1 the schematic arrangement of the focimeter is shown. If there is no test lens in place, a target T initially placed at the front focal point F_C of the collimator lens is imaged in focus through the telescope. A lens now placed in front of the telescope will de-collimate the beam and the image of the target will now be out of focus in the telescope. To refocus the target, it can be moved along the optical axis of the collimator. The image will be a distance x' from the back focal point of the collimating lens, if the target has to be moved a distance x towards or away from the collimator to refocus it. The vertex power is related to the target displacement x on a linear scale, which because of its linearity can be easily calibrated. (Smith, Atchison 1997)

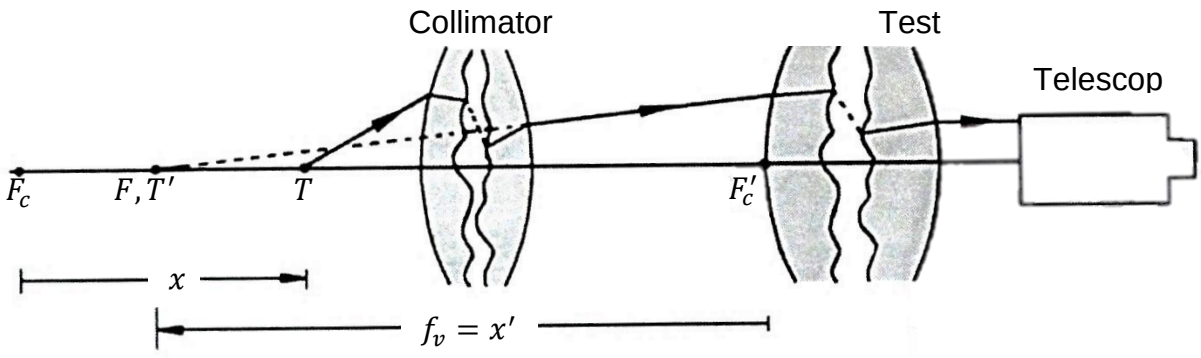

Fig. 1: The focimeter (Smith, Atchison 1997).

Focimeters can be divided in visual, projection or fully automatic. The visual type is already shown in figure 1, the image of a target $\boldsymbol{T}$ is viewed and focused through an optical system that consists basically of a collimator and a viewing telescope. The scale reading may also be located in the eyepiece of the telescope. The telescope is replaced by an optical system in the projection type, projecting the image of the target onto a viewing screen. The operator has to make some judgment on the best

focus of the target in both types of instruments. In contrast, the instrument automatically locates the optimum focus and the final powers are given directly on some type of display in automatic instruments. (Smith, Atchison 1997)

2.2 Optical Aberrations

Geometric optics describe light as rays. This model provides rules for the propagation, reflection and refraction of light through optical systems such as lenses or mirrors. It is possible for any system to calculate exactly one focal point P' where the rays focus being converged or diverged by it. Reality is more complicated. Any influences which deteriorate that focal point and change the scale or the color are called aberrations. (Nolting, Wassmer 2001; Marchesi 2011; Hecht 2002; Chauhan, Varma 2009; Zeiss 2000)

Aberrations can be divided in two groups. The first one is caused by the multichromatic nature of light itself and is called chromatic aberration. A difference is only made between axial and lateral aberration. The second one is called monochromatic aberration and results from traversing light rays through an optical system. Some types of aberration such as Defocus, Spherical Aberration, Coma and Astigmatism blur the focal point. Others, such as Field Curvature and Image Distortion impact the focal plane. (Hecht 2002)

Not all optical aberrations are relevant for this thesis but for the sake of completeness all first order aberrations are named and described. Important and relevant are field curvature, astigmatism and refraction error.

2.2.1 Chromatic Aberrations

A lens' refraction power and therefore the focal length is given by the lensmaker's equation:

$$\frac{1}{f} = (n_l - 1) \cdot \left(\frac{1}{R_1} - \frac{1}{R_2}\right) \qquad \text{EQ 1}$$

The refractive index $n_l(\lambda)$ is a function of the wavelength λ and so the focal length *f* is also dependent on the wavelength. (Hecht 2002) White light propagating through a prism is dispersed into its components. Blue light with a short wavelength is deviated through a higher angle than red light with a long wavelength, in-between the prismatic colors can be seen: red- orange- yellow- green- blue- purple. (Nolting, Wassmer 2001; Hecht 2002)

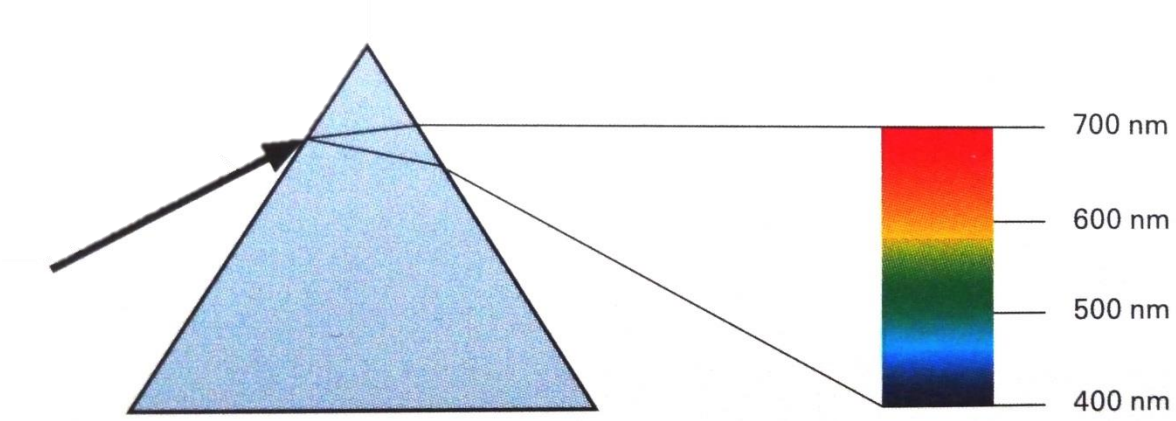

Fig. 2: Dispersion of white light into its spectrum by a prism (Marchesi 2011).

When white light of a multichromatic source propagates through a lens, the same concept of dispersion leads to chromatic aberration. (Hecht 2002)

J. v. Fraunhofer occupied himself with dispersion, too. He wanted to measure the refractive indexes of different types of glass for a defined wavelength. He discovered at the dispersion of sunlight, that there are not all prismatic colors to be seen. His conclusion was that in the spectrum of sunlight there are some wavelengths missing. Thus these lines were named Fraunhofer lines and he labeled them with letters. Today it is known that gases in the sun's atmosphere absorb those components of the sunlight. To identify a spectral color, today the Fraunhofer lines of the sunlight's spectrum are used no more, but the specific lines produced by spectral lamps. (Nolting, Wassmer 2001; Marchesi 2011)

Table 1: Standard wavelengths.

Element	Wavelength in nm	Color of the light	Name given by Fraunhofer
Cadmium	479.99	blue	F'
Quicksilver	546.07	green	e
Cadmium	643.85	red	C'

Table 1 shows the standard wavelengths which are relevant for the calculation of the Abbe number ν. The definition is:

$$\nu_e = \frac{n_e - 1}{n_{F'} - n_{C'}} \qquad \text{EQ 2}$$

The Abbe number is a constant to categorize the image quality of a lens in terms of chromatic aberration. The difference of the refraction indexes $n_{F'}$ and $n_{C'}$ (for cadmium with the wavelengths of 479.99 nm and 643.85 nm) is called principal

dispersion and n_e is the fraction index for light of a mercury spectral lamp at the wavelength of 546.07 nm. A high Abbe number indicates low dispersion; the other way round a low Abbe number causes high dispersion. (Nolting, Wassmer 2001; Marchesi 2011)

2.2.1.1 Axial Chromatic Aberration

As illustrated in the previous chapter the lensmaker's formula shows the dependence of a lens' focal length on the wavelength of the incident light. Hence polychromatic light does not result in one focal point, but each component of the incident light causes an own specific focal point. This phenomenon is called axial or longitudinal aberration. (Nolting, Wassmer 2001; Hecht 2002)

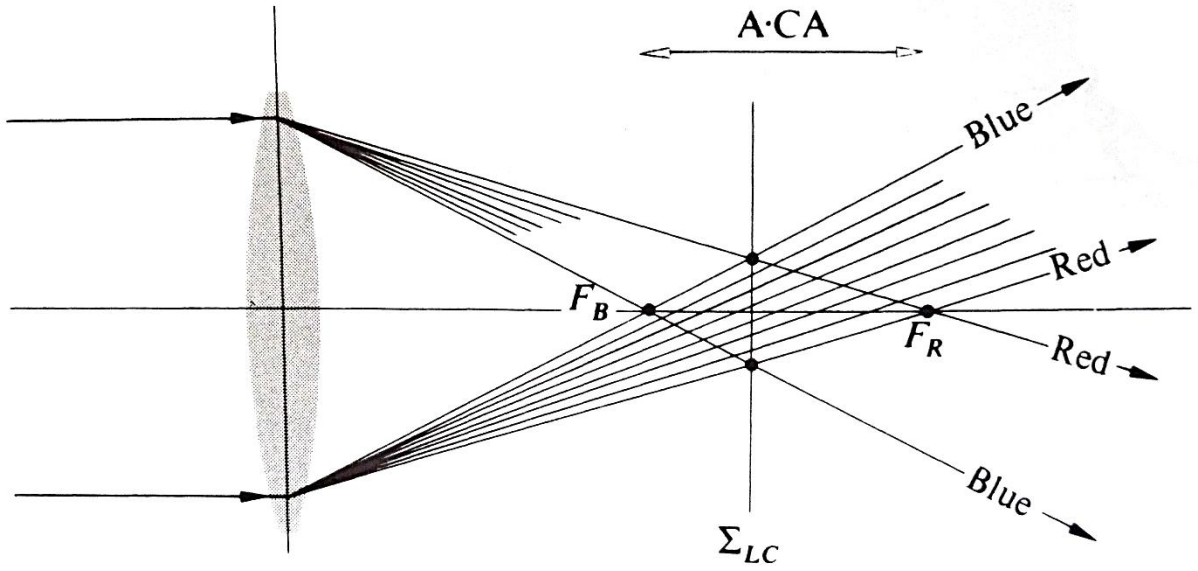

Fig. 3: Axial chromatic aberration *A·CA* for red and blue light (Hecht 2002).

The figure 3 shows the location of the circle of least confusion (See chapter 2.2.2.5, Astigmatism, p. 14) in the plain Σ_{LC}. For the human eye the sharpest picture will appear there between the focal points F_B for blue and F_R for red light. (Hecht 2002)

2.2.1.2 Lateral Chromatic Aberration

An off-axis point gets imaged due to the principle of dispersion:

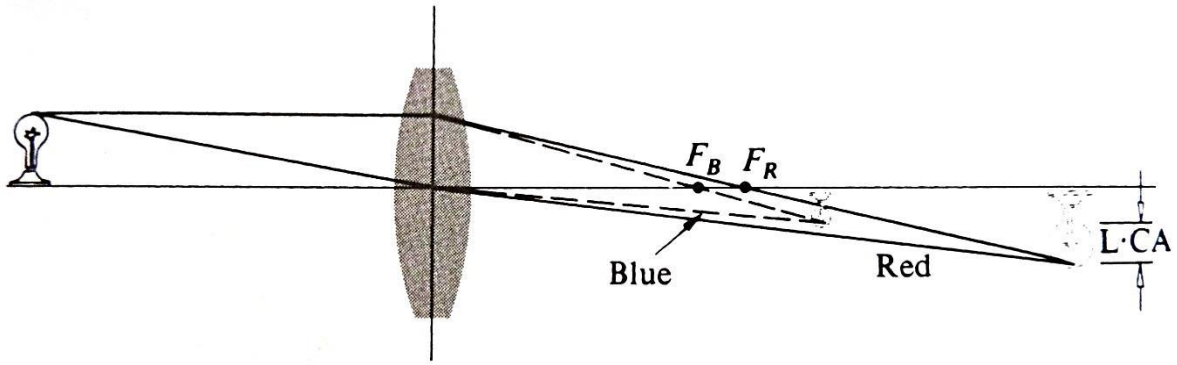

Fig. 4: Lateral chromatic aberration *L·CA* for red and blue light (Hecht 2002).

Figure 4 illustrates the transverse magnification which also depends on the wavelength λ. That fact is caused by the focal length's f reluctance to the wavelength λ of the incident light (already shown in chapter 2.2.1, Chromatic Aberrations, p.3). The lateral chromatic aberration $L \cdot CA$ is the difference of the two pictures which appear due to the highest (for blue light with focal point F_B) and lowest (for red light with focal point F_R) refraction. (Hecht 2002, 2009; Nolting, Wassmer 2001; Zeiss 2000)

Figure 4 shows lateral chromatic aberration for red and blue light. If there is a multichromatic light source, each component of the incident light creates one image with a defined focal length. In summary, the resulting image consisting of many overlapping pictures appears out of focus and with slight color fringes at the edges. (Hecht 2002; Nolting, Wassmer 2001; Marchesi 2011)

2.2.2 Monochromatic aberrations

As per first-order or Gaussian theory the focal length f of a breaking interface is defined as:

$$\boldsymbol{f = \frac{n_1}{n_2 - n_1} \cdot R} \qquad \textbf{EQ 3}$$

The refractive indexes $n_1$and $n_2$are the ones before and after the surface, *R* is the radius of the refractive interface. But the validity of this theory ends with abaxial rays, it is no complete accurate model. To include rays which come from the extremities of a lens one has to consider the five third-order aberrations: spherical aberration, coma, astigmatism, field curvature and image distortion. They first were surveyed by Philip Ludwig von Seidel and consequently named after him. Besides the Seidel Aberrations, there are aberrations of higher order, but this paper only treats the five third-order aberrations. (Hecht 2002)

2.2.2.1 Spherical Aberration

Gaussian theory defines one focal point *F'* for a lens. Reality shows that paraxial rays which pass through a converging lens with a height *h* are bent stronger and therefore cross the optical axis in front of the paraxial focus. So the focal length is not only dependent on the wavelength of the incident light, but even for monochromatic light there are different focal points for different heights of incidence. Adverse to the shown positive spherical aberration, there is negative aberration for diverging lenses. The marginal rays cross behind the paraxial focal point. Spherical aberration is defined in two ways. (Marchesi 2011; Nolting, Wassmer 2001; Hecht 2002)

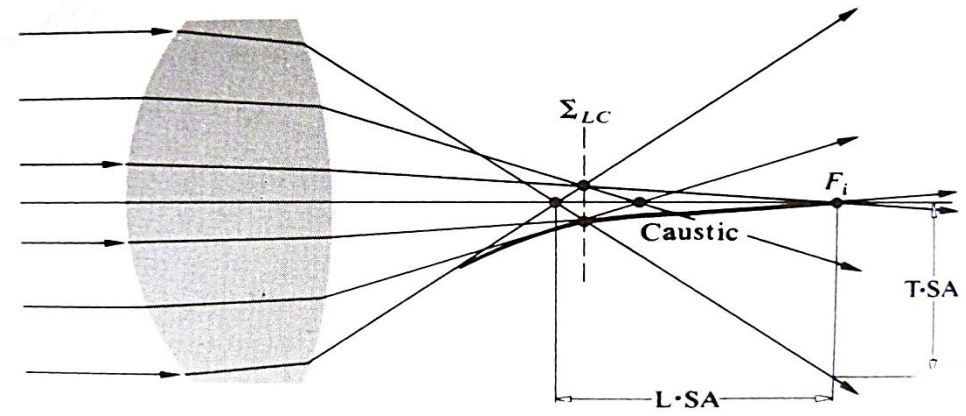

Fig. 5: Spherical aberration for a lens (Hecht 2002).

The longitudinal spherical aberration $L \cdot SA$ is the segment between the focus *F'* and the focal point of the marginal rays which focus farthest. The height of the marginal rays at the focal plane is called longitudinal spherical aberration $T \cdot SA$. The point where the marginal rays and the caustic (this is the envelope of the refracted rays)

cross, locates the circle of least confusion Σ_{LC}. (Hecht 2002) (Marchesi 2011; Nolting, Wassmer 2001; Hecht 2002)

Especially in photography, the spherical aberration is also called aperture aberration due to the dependence of the incidence height and therefore the aperture value. The smaller the aperture is chosen the higher the depth of focus increases. (Marchesi 2011)

Besides the incidence height of the marginal rays also refractive power and shape of a lens influence the spherical aberration. Nolting and Wassmer have shown for a spherical converging lens with a radius of 40 mm that height and angle of incidence are dependent. (Nolting, Wassmer 2001)

Table 2: Height and angle of incidence in relation for a lens with radius 40 mm.

Height of incidence *h*	0,3 mm	3 mm	30 mm
Angle of incidence ε	0,43°	4,3°	48,59°

It is not possible to correct spherical aberration completely, but there are several ways to minimize it. For spectacle optics the aspherical design of a lens is the most important one. “Optical elements (lenses and mirrors) […] with one or both surfaces neither planar nor spherical, are referred to as aspherics.” (Hecht 2002) That means that a lens’ radius differs and increases towards the edges. Therefore the angle of incidence gets lower and the spherical aberration is reduced. (Hecht 2002; Nolting, Wassmer 2001)

2.2.2.2 Coma

When an object point lies even a short distance from the axis, Coma, or chromatic aberration, an image-degrading, monochromatic, primary aberration can be observed. This phenomenon is caused by the fact that principal planes can actually be treated in the form of planes only in the paraxial region. Actually, they are curved surfaces. A parallel bundle of rays will focus at one axial point F_i, a distance of one focal length back from the rear vertex. Yet the resulting focal lengths and thus the transverse magnifications will differ for the rays traversing off-axis regions of the lens. When the image point is on the optical axis, this situation is of little consequence, but when the ray bundle is oblique or the object point is off-axis, coma will be observed.(Hecht 2002)

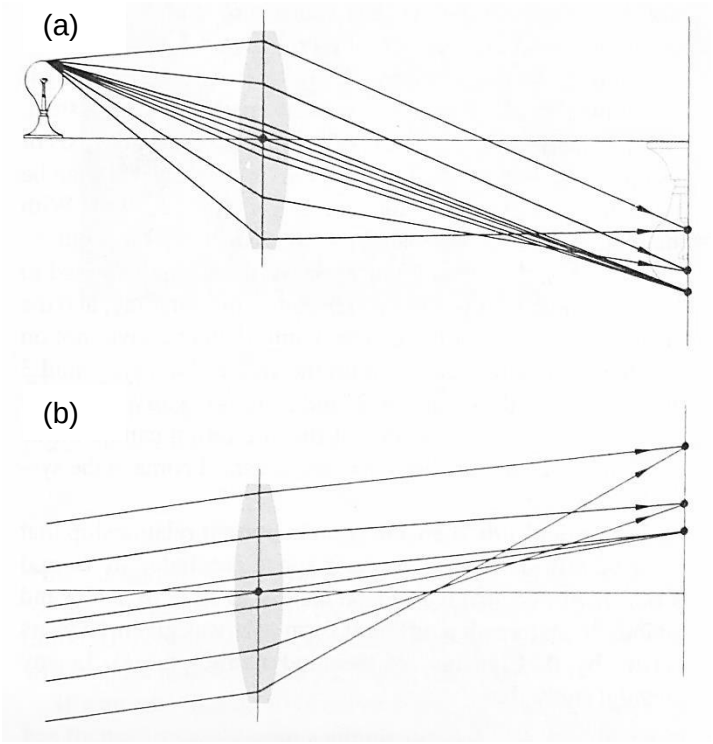

Fig. 6: Positive coma (b) and negative coma (a) (Hecht 2002).

A comparison of negative and positive coma can be seen in figures 6 (a) and (b). The transverse magnification M_T depends on *h*, the ray's incident height at the lens that is shown in figure 6 (a). Meridional rays traversing the edges of a lens arrive at the image plain closer to the axis than do the rays close to the ray, which passes through the principal points. Hence the coma is negative because the least magnification is associated with the marginal rays that would form the smallest image. In contrast, the coma in figure 6 (b) is positive because the marginal rays focus farther from the axis than the principal one. (Hecht 2002)

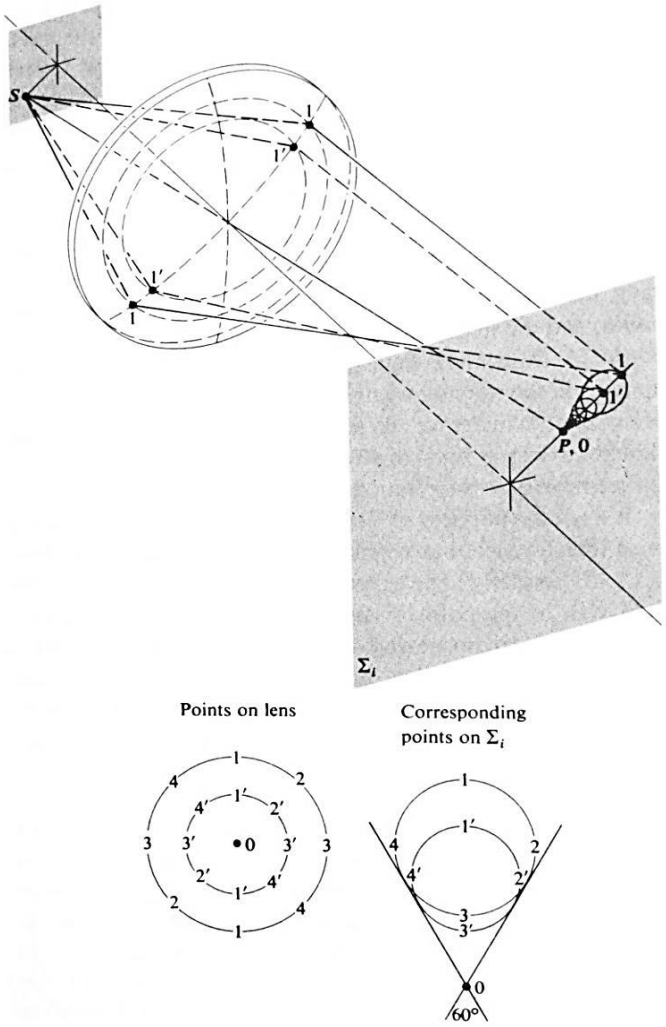

Fig. 7: The geometrical coma image of a monochromatic point source. The central region of the lens forms a point image at the vertex (Hecht 2002).

To illustrate the comatic imaging of an off-axis object point *S*, several skew rays are drawn in figure 7. Each circular cone of rays whose endpoints form a ring on the lens is imaged in a chromatic circle on the plane Σ_i. In this case, positive coma is presented, so a larger distance of the comatic circle from the axis is caused by a larger ring on the lens. When the outer ring is created by marginal rays, tangential coma is defined as the distance from 0 to 1 in the image, and the length from 0 to 3 on Σ_i is termed the sagittal coma. The main image with little more than half of the energy appears in the roughly triangular region between 0 and 3. Because of its asymmetric configuration, the coma image, which is named after its cometlike tale, is often thought to be the worst of all aberrations. (Hecht 2002)

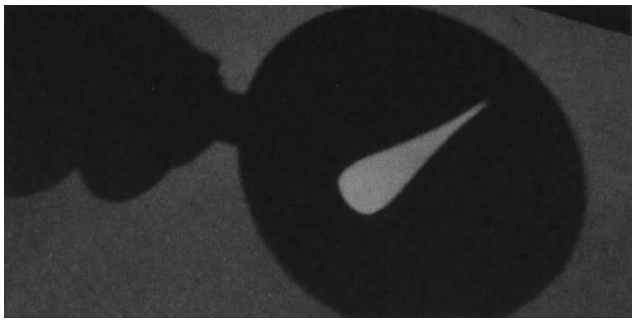

Fig. 8: Coma image generated by a loupe hold in a lightly inclined position (Nolting, Wassmer 2001).

It's an easy matter to observe coma while focusing sunlight with a simple loupe. To make an angle with the optical axis, one has to tilt of the lens slightly, so that the nearly collimated rays from the sun will cause the focused spot to flare out into the characteristic comet shape. (Hecht 2002; Nolting, Wassmer 2001)

2.2.2.3 Image Distortion

Distortion is another of the five primary, monochromatic aberrations which are treated in this paper. It is caused by the transverse magnification M_T, being a function of the off-axis image distance y_i. Paraxial theory predicts a constant M_T, but that distance may differ. In simple terms, distortion arises of the optical property of a lens: different areas of the lens have different focal lengths and different magnifications. In the absence of any other aberrations, distortion will be observed in a misshaping of the image as a whole, even though each area of the image is sharply focused. Figure 9 shows an undistorted object in comparison to a positive or pincushion-distorted and a negative or barrel-distorted square array. When suffering positive distortion, each image point is imaged radially outward from the center, therefore M_T increases with y_i. Similarly, negative distortion correspondents to the situation in which each point on the image moves radially inward toward the center with M_T decreasing with the axial distance. (Hecht 2002)

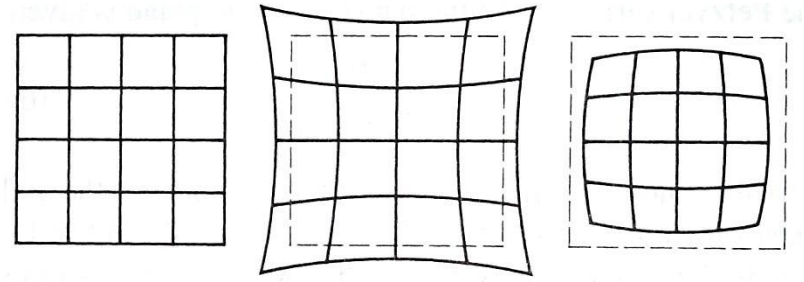

Fig. 9: An undistorted object in comparison to a pincushion- and barrel-distorted object (Hecht 2002).

Distortion can easily be illustrated by just taking a look through an aberrant lens at a piece of squared paper. Usually, thin lenses will show no distortion, whereas negative or positive, thick, simple lenses will suffer positive or negative distortion, generally. (Hecht 2002)

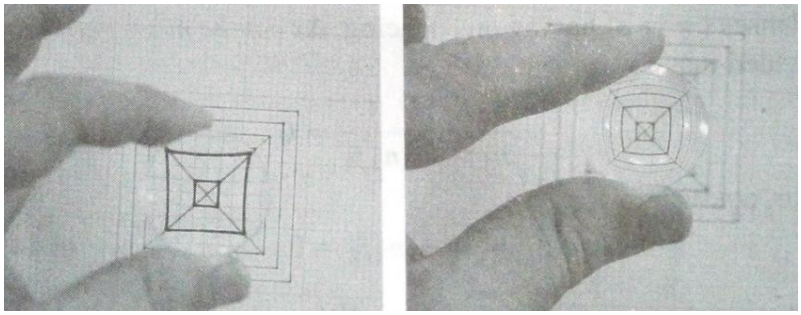

Fig. 10: When the magnification on the optical axis is less than the off-axis magnification, pincushion distortion results. When it's greater on axis than off, barrel distortion results, both demonstrated with a single thin lens (Hecht 2002).

2.2.2.4 Field Curvature

If there were an optical system free of all the aberrations thus far considered, between points on the object and image surfaces there would then be a one-to-one correspondence, a so called stigmatic imagery. A planar object perpendicular to the axis will be imaged as a plane only in the paraxial region. At finite apertures the image results in a curved stigmatic surface and is a manifestation of the primary aberration known as Petzval field curvature, after the Hungarian mathematician Max Petzval (1807-1891). The effect can be appreciated by examining figure 11. An object σ_0, which is a spherical segment, is imaged by the lens as a spherical segment σ_i both centered at O. Flattening out σ_0 into the plane σ_e will move each image point toward the lens along the concomitant chief ray, forming a paraboloidal Petzval surface Σ_p. A Petzval surface for a positive lens curves inward toward the object plane, in contrast it curves outward away from the plane for a negative lens. A combination of positive and negative lenses can negate field curvature. (Hecht 2002)

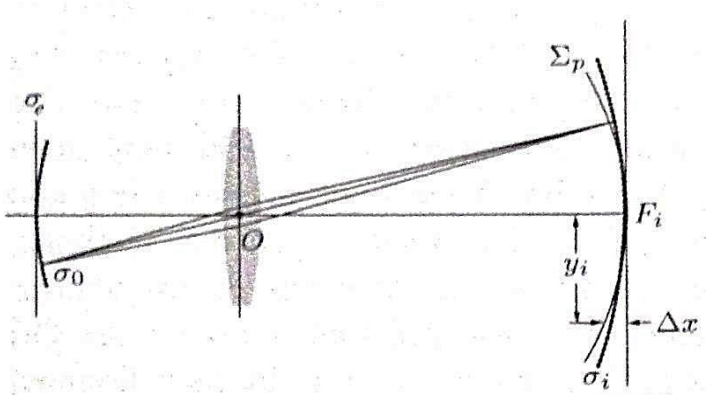

Fig. 11: When the object corresponds to σ_e, the image will correspond to Σ_p (Hecht 2002).

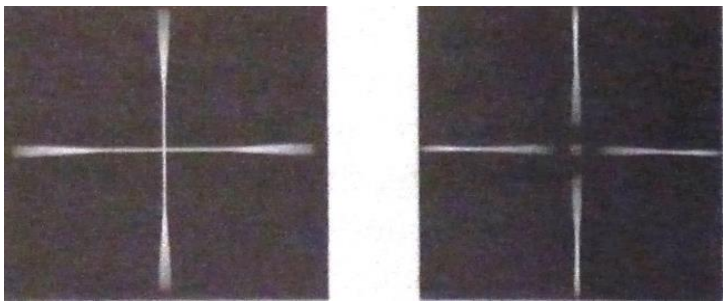

Fig. 12: The image formed on a flat screen near the paraxial image plane will be in focus only at its center. Moving the screen closer to the lens will bring the edges into focus (Hecht 2002).

2.2.2.5 Astigmatism

Another third primary aberration which is relevant for the measurements of this thesis is known as astigmatism and appears due to oblique incident rays when an object point lies off axis. Astigmatism comes from the Greek words a- and stigma which mean no spot or point. To facilitate its description, the meridional or tangential plane is defined by the chief ray passing through the center of the aperture and the optical axis. The sagittal plane is then upright to the meridional plane and contains the chief ray. The sagittal plane is unbroken from one end of a complicated lens system to the other, the sagittal plane in contrast generally changes slope as the chief ray is deviated at the different elements. Hence it is possible to speak of several sagittal planes, one for each region within the system. All skew rays from the object point lying in a sagittal plane are still named sagittal rays. (Hecht 2002; Smith, Atchison 1997)

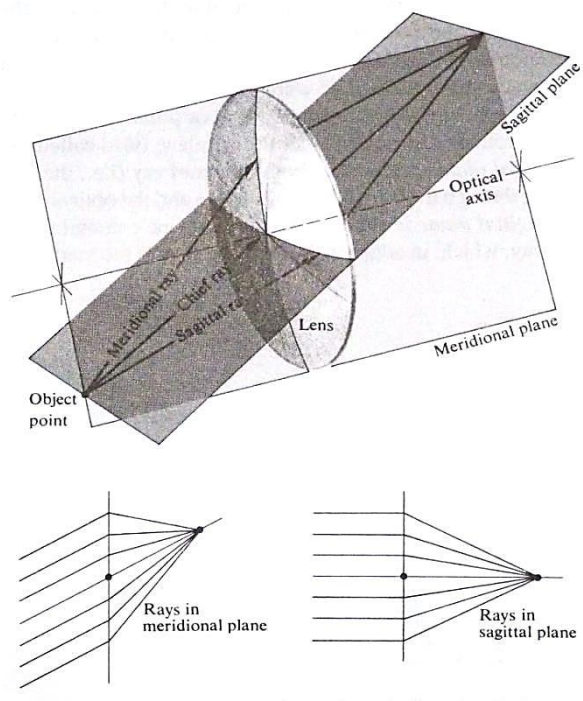

Fig. 13: The sagittal and meridional planes (Hecht 2002).

There is no need to make a distinction between meridional and sagittal planes if there is an axial object point, because a spherical surface of a lens creates a symmetrical cone of rays. In all planes enclosing the optical axis the ray configurations are identical. Without spherical aberration, all areas of the lens have the same focal length and consequently all rays cross at one defined focus. Unlike the shown case, the configuration of an oblique, parallel ray bundle differs in the meridional and sagittal planes, as do the focal lengths in these planes. Here the

meridional rays are tilted more with respect to the lens and have a shorter focal length than the sagittal ray. The focal length difference depends on the lens' power and the angle of incidence. This so called astigmatic difference increases as the object point moves from the axis and therefore the obliqueness of the rays becomes higher. It is zero, if the object lies on the optical axis. (Hecht 2002)

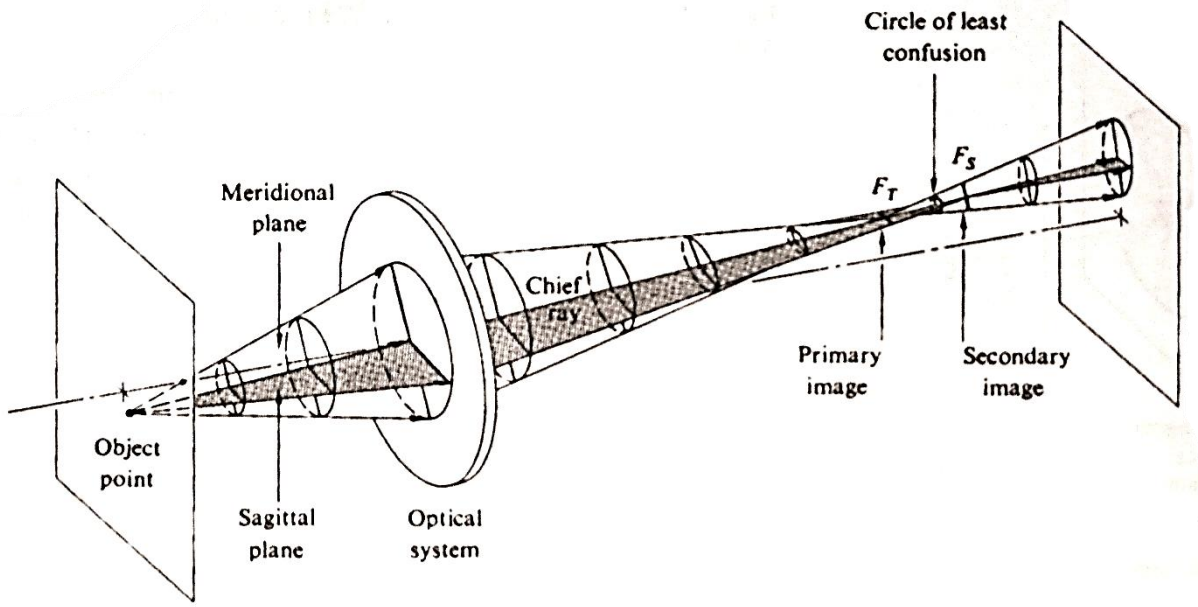

Fig. 14: An off-axis point is imaged by a lens due to aberrational astigmatism (Hecht 2002).

The incident conical bundle of rays takes on an altered form after refraction, because of the two different focal lengths. The cross section of the beam is circular when it leaves the lens, but it gradually becomes elliptical with the major axis in the sagittal plane, until at the tangential or meridional focus F_T, the ellipse seems to form a line which is known as the primary image (see fig. 14). After all rays from the object point have traversed this line, the beam's cross section rapidly opens out until it is again circular and forms the circle of least confusion. Farther from the lens, cross section of the beam again deforms into a line. This time this secondary appears at the sagittal focus F_S in the meridional plane. (Hecht 2002)

The astigmatic difference increases as the object moves farther off-axis. This leads to an increasing circle of least confusion in diameter, therefore the image will deteriorate, losing definition around its edges. The secondary line image will always point toward the optical axis but change in orientation with changing object position. The primary line image will also vary in orientation, but will remain perpendicular to the secondary image. (Hecht 2002; Smith, Atchison 1997)

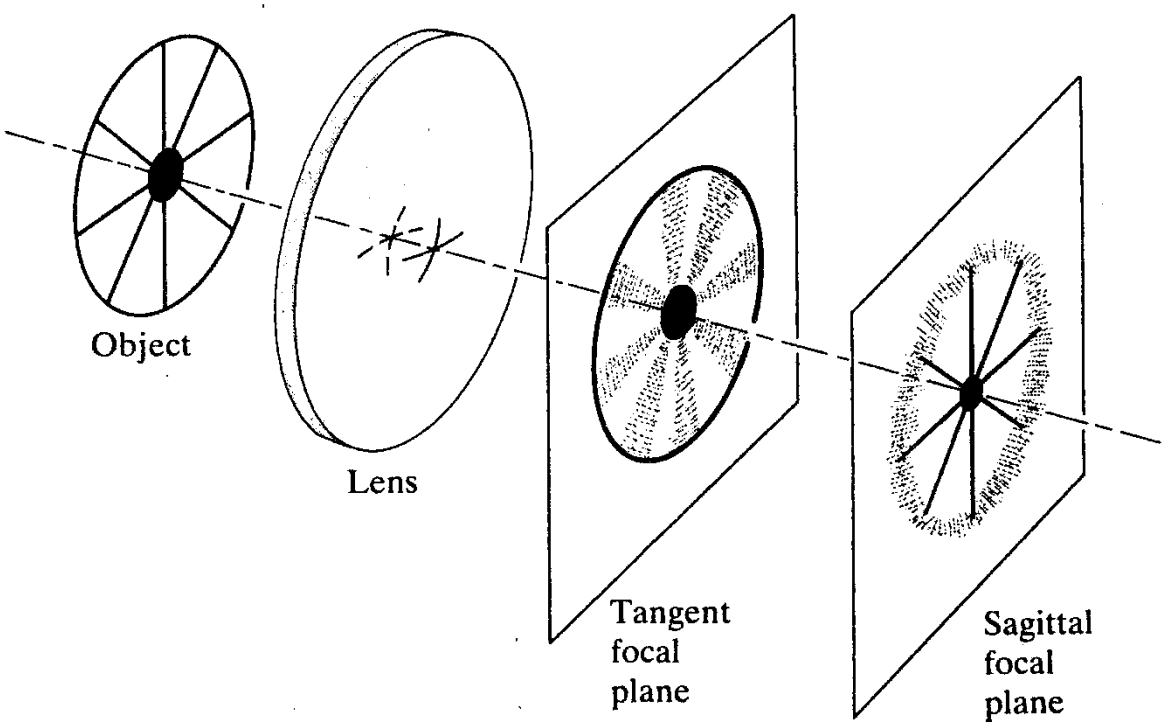

Fig. 15: Images in the tangent and sagittal focal planes (Hecht 2002).

An interesting effect caused by this arrangement is shown in figure 16 when the object consists of radial and tangential elements. The primary and secondary images are formed of transvers and radial dashes, which increase in size when the distance from the axis also increases. In the last case, the dashes point toward the center of the image–thus they are called sagitta. (Hecht 2002)

2.2.2.6 Image surfaces and refraction error

Astigmatism and field curvature are intimately related. In the presence of astigmatism there are two paraboloidal image surfaces, the tangential Σ_T and the sagittal Σ_S (see fig. 16). The loci of all the primary and secondary images are located on these surfaces (as the object point roams over the object plane).

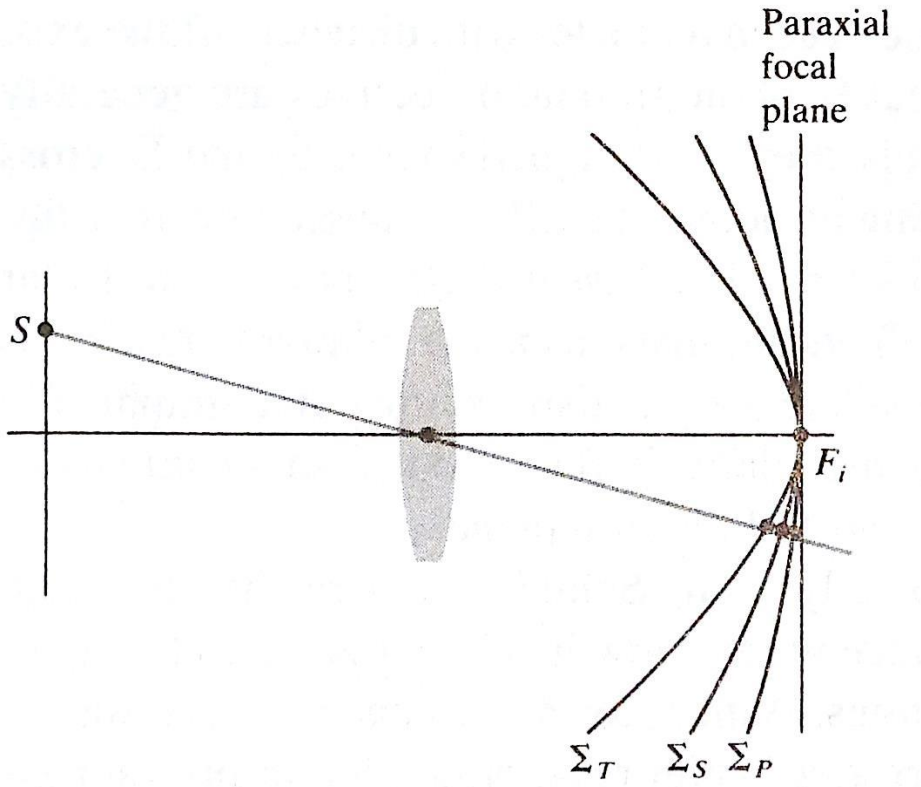

Fig. 16: The tangential, sagittal and Petzval surfaces (Hecht 2002).

At a given height y_i, a point on Σ_T always lies three times as far from Petzval sphere as does the corresponding point on Σ_S, and both are on the same side of Σ_P (see Fig. 16). If there is no astigmatism, Σ_S and Σ_T coalesce on Σ_P, which differs from the far point sphere. This angle-dependent defocussing is called refraction error. It can't be annulled because the Petzval surface cannot be corrected into the far point sphere. (Hecht 2002; Diepes; Blendowske 2002)

2.2.3 Optical Aberrations' Evaluation

Comparing an eye's aberrations to the optical aberrations of an ophthalmic lens the axial aberrations (axial chromatic aberration and Spherical aberration) are negligible small. Spherical aberration is very small due to narrow pencils of rays. Even when the diameter of the eye' pupil expands, the eye's spherical aberration is higher than the lenses' is. Axial chromatic aberration of an ophthalmic lens, anyway

uncorrectable with one lens, is much smaller than for a human eye (at least 1 dpt axial chromatic aberration).

Off-axis aberrations, named below, are partially more relevant.

- lateral chromatic aberration
- coma
- astigmatism
- field curvature
- image distortion

These occur with higher angles of incidence. In this paper a rotatable measuring device around an imaginary center of rotation is evaluated. Therefore angles of incidence up to 20° occur and the off-axis optical aberrations gain importance. Lateral chromatic aberration can only be reduced, not corrected with one lens by a change in material. Coma is also negligible small because the pencils of rays are narrow. Those two are not of interest and are not further regarded. Neither field curvature nor image distortion is correctable with normal ophthalmic lenses. In this paper astigmatism is computed on x- and y-axis of a lens, distortion is to be observed 45° to those axis. Therefore distortion is also irrelevant.

Eventually the relevant optical aberrations for this paper are:

- Astigmatism (and refraction error)
- Field curvature

These two are considered further. The tangential and sagittal oblique vertex sphere powers caused by astigmatism are calculated with reference to the vertex sphere for a +4 dpt spherical lens with an incidence angle of 20° in chapter 5.1, CalculationTo validate the measured values, these are compared to a calculation. This is shown in the next chapter.

Calculation. (Diepes, Blendowske 2002; Smith, Atchison 1997)

3 Measuring Setup

3.1 Description of used focimeters

3.1.1 Huvitz HLM–7000 Automatic Lensmeter

The focimeter manufactured by Huvitz has various functions; the relevant ones are described in this chapter. The HLM–7000 was used in this work.

The HLM – 7000 is a full automatic digital focimeter, using the Hartmann–Shack–principle. For a general overview of the operating mode of a focimeter see chapter 2.1, Focimeter. The HLM–7000's measurement range of the back vertex power is between ±25 dpt, the range of cylinder power between ±10 dpt and the axis is given in 1°-steps between 1° to 180°. The output values are selectively graduated in 0.01 dpt, 0.12 dpt or 0.25 dpt steps which are presented on a color display. The aperture pupil is adjustable and the diameter may be lessened by switching from glasses-mode to contactlens-mode.

A Shack–Hartmann (or Hartmann–Shack) wavefront sensor is an optical instrument that is used to characterize an imaging system. An array of lenses (called lenslets) of the same focal length is focused onto a photon sensor. From the position of the focal spot on the sensor then the local shift of the wavefront across each lens can be calculated. Any phase aberration can be approximated to a set of discrete shifts. All of these tilts can be measured by sampling an array of lenslets, the whole wavefront approximated and therefore the power of a lens calculated. (Wikipedia 2014)

The Huvitz HLM–7000 Automatic Lensmeter was used with the following adjustments:

Table 3: Adjustments of the HLM–7000 for test measurements.

Menu item	Submenu	Explanation
Lens	Normal	Single vision lens
Cylinder	-	Presentation of cylinder in minus
BPS	9600	Speed of the interface
Step	0.01	Increment of display in 0.01 dpt
Auto R/L	On – S/R/L	Switches on the automatic right/left single glass function
Prism	P – B	Display of prisms in terms of value and direction

ABBE	Normal	
Wavelength	e-line	Reference wavelength is mercury (e-line at 546,07nm)
EP	8 mm	Entrance pupil
RS 232C	LMTORK (old)	Switches on the communication between HLM and HRK, MRK and CDR, HDR series
Beep	Off	Acoustic signal tone off
PD	Off	Pupil distance measurement
Prism Step	0.01	Increment of display in 0.01 dpt
Printer	Off	Possibility to print off
Auto Printer	Off	Automatic printing off

3.1.2 Tomey TL–3000A

The TL–3000A also is a full automatic focimeter with an implemented Hartmann–Shack–Sensor. The reading can be printed. Basically, it works the same way than the Huvitz HLM–7000. The display to present the results is not in color. Apart from that the measuring ranges (refractive power ±25 dpt and cylindrical power ±10 dpt) and the way of presentation are adequate.

Table 4: Adjustments of the TL–3000A.

Menu item	Submenu	Explanation
Lens	Single vision	Single vision lens
R–L	S-mode	For measuring single lenses
PD	OFF	Pupil distance is not measured
+ <-> -	-	Cylinder reading in minus
Step	0.01	Increment of display in 0.01 dpt
Print	Off	No printing
PRISM	NON	No prism measured
Beep	Off	Acoustic signal tone off

3.2 Measuring Arrangement

A measuring device was made to be mounted on the Huvitz HLM–7000 Automatic Lensmeter. In 2013 this measuring device was constructed and created by Aalen University's laboratory supervisor in optometry, Reinhard Liebhäußer in accordance with the center of rotation of the eye. This principle is described in the following passage for a human eye.

Three pairs of muscles control the eye's direction of gaze; one pair lying in the horizontal plane for rotation about a vertical axis, one pair in the vertical plane for rotation about a horizontal axis and a third pair of torsional muscles for rotation of the eye about the optical axis. We assume that these three axes intersect and the point of intersection is called the center of rotation of the eye Z'. (Smith, Atchison 1997)

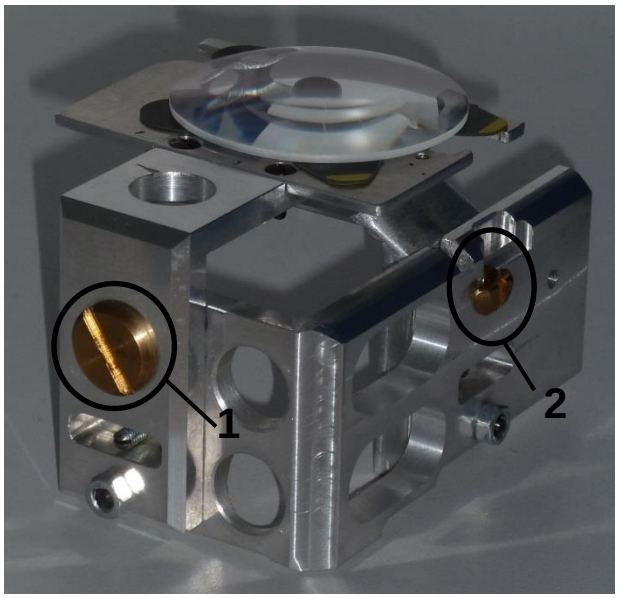

Fig. 17: The rotatable measuring device simulates the center of rotation of the eye, rotating about the x-axis (golden screw number 1) and y-axis (golden screw number 2).

The device has a lens tube designed with a diameter of 8 mm which allows attachment to the focimeter (see fig. 21). This tube is the entrance pupil of the optical system. To fix an ophthalmic lens adhesive pads are used. The lens can then be centered to the visual center of the focimeter.

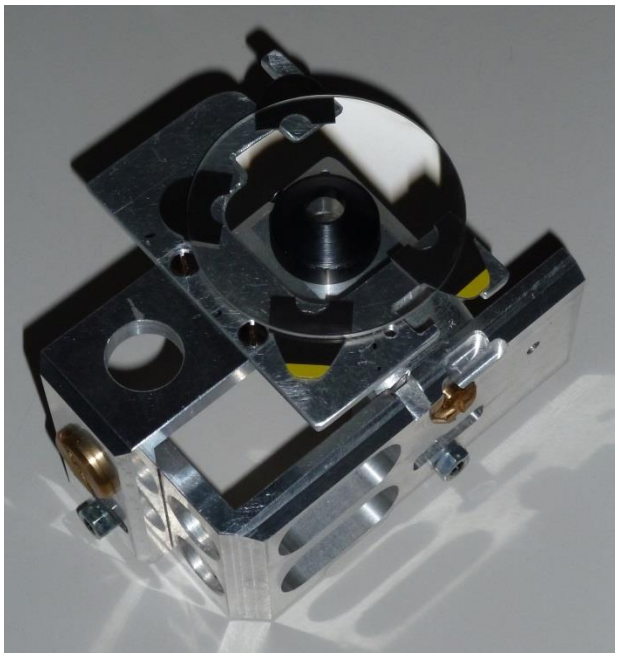

Fig. 18: Mounted ophtalmic lens on the measuring device.

The device is attachable to the Huvitz HLM–7000 and also to the Tomey TL–3000A. It can be tightened with screws to the Huviz and we used adhesive pads to attach it to the Tomey focimeter (see Fig. 23).

Fig. 19: Tomey TL–3000A lensmeter with applied measuring device and mounted lens.

The device and the lens is rotatable in 5° steps to four directions (left, right, up and down). Hence the measurements are reproducible. There is the possibility to rotate the device from the basic adjustment of 0°/0° in four directions (on x-axis see Fig. 17: golden screw number **1** as the axis of rotation, and y-axis see Fig. 17: golden screw number **2** as the axis of rotation, each negative and positive) with four steps of 5° where the maximum is reached at +/- 20°. The results of measurement can be illustrated in matrixes of 9 x 9 fields (each field represents one measurement point at the lens, i.e. 40° respectively on x- and y-axis). A rotation of 5° of the device is comparable to a shift of approximately 2.6 mm at a glass.

The power of a spectacle lens depends amongst others on the corneal vertex distance e between the lens and the eye. A change in this distance results in a change of refractive power. A correlation of a lens' equivalent power $S'_{\infty 1}$ in vertex distance e_1 and the power $S'_{\infty 2}$ in distance e_2 is given by the following equation.

$$S'_{\infty 2} = \frac{S'_{\infty 1}}{1+(e_2-e_1)S'_{\infty 1}} \qquad \textbf{EQ 4}$$

The distance b' is not directly measureable, but has to be calculated for each lens from the device's radius of rotation $r_{rotation}$, the offset z (between the tube's front and the front of the adhesive pads which are attached to the seating surface of the measuring device) and the distance s of a mounted ophthalmic lens (s differs for each lens, for a calculation see chapter 5.1, CalculationTo validate the measured values, these are compared to a calculation. This is shown in the next chapter.

Calculation).

$$b' = r_{rotation} - z + s \qquad \text{EQ 5}$$

Fig. 20 illustrates the correlation.

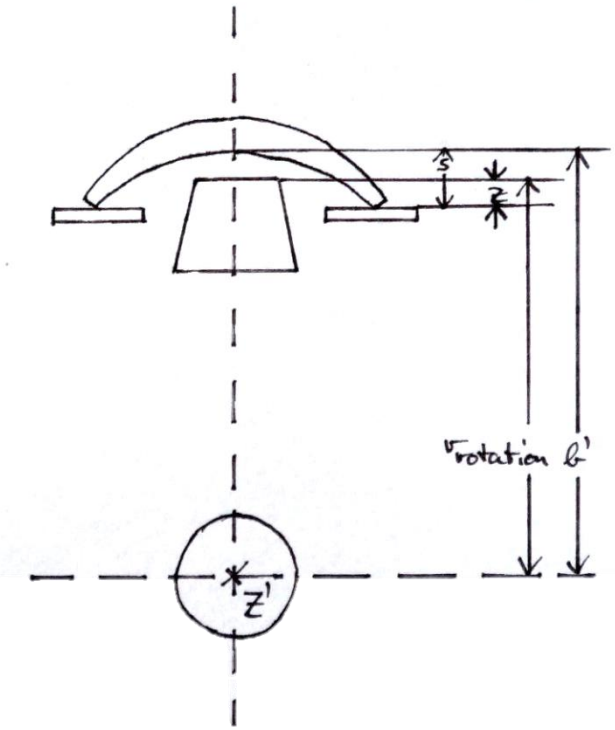

Fig. 20: Schematic correlation of the device's radius of rotation $\mathbf{r_{rotation}}$, the offset $\mathbf{z}$ (between the tube's front and the front vertex of the adhesive pads) and the distance $\mathbf{s}$ of a mounted ophthalmic lens.

The resulting b' equates to the distance between the center of rotation of the eye Z' and the back vertex of a lens. On average it amounts 30 mm for the technical device. Due to Gullstrand Z' lies 13.5 mm behind the cornea, therefore the vertex distance of the measuring device is 30 mm-13.5 mm=16.5 mm. Table 5 shows the consequences of a variating vertex distance.

Table 5: Lenses' different equivalent powers for different vertex distances.

	S'_∞ [dpt]	e [mm]	S'_∞ [dpt]	e [mm]
Measuring device	-5.00	16.5	+4.50	16.5
Normal vertex distance	-4.89	12.0	+4.59	12.0
FocusSpecs	-4.80	8.0	+4.68	8.0
Measuring device	-10.00	16.5	+10.00	16.5
Normal vertex distance	-9.57	12.0	+10.47	12.0
FocusSpecs	-9.22	8.0	+10.93	8.0

With increasing vertex distance the lens' magnitude in vertex power also increases. The following values for b' were calculated for the four lenses (for calculation see chapter 6).

Table 6: Values of b' for the four test lenses.

S'_∞ [dpt]	+4 (spherical)	+4 (aspherical)	-4 (spherical)	-4 (aspherical)
b [mm]	28.9	28.3	33.3	30.5

The measured data was recorded manually with Excel. It covered fields of 9x9 measuring points and is presented in matrixes in the following.

3.3 Test measurements

To validate the measuring device (see chapter 3.2, Measuring Arrangement), four lenses were used. Those were two lenses of +4 dpt and two lenses of -4 dpt respectively in spherical and aspherical design. In the beginning a +6 dpt aspheric lens was attached to the device for a first test measurement. The results of the measurement are presented below:

Table 7: Spherical power of a +6 dpt aspherical lens.

10,76	8,57	7,42	6,92	6,75	6,88	7,34	8,36	10,43
8,49	7,09	6,48	6,08	6,03	6,06	6,41	6,99	8,33
7,45	6,46	6,03	5,96	5,98	5,95	6,00	6,38	7,24
6,96	6,09	6,00	5,96	5,96	5,96	5,94	6,03	6,77
6,83	6,06	5,99	5,97	5,96	5,96	5,96	6,02	6,69
6,98	6,09	5,97	5,99	5,97	5,94	6,00	6,04	6,78
7,46	6,47	6,02	5,96	5,96	5,96	6,00	6,16	7,19
8,54	7,06	6,44	6,07	6,03	6,06	6,18	6,87	8,08
10,35	8,32	7,30	6,85	6,71	6,81	7,19	8,10	9,72

The spherical power is 6.78 dpt in average, the standard deviation amounts 1.10 dpt.

Table 8: Cylindrical power of a +6 dpt aspherical lens.

-3,26	-1,92	-1,18	-0,81	-0,66	-0,75	-1,09	-1,82	-3,18
-1,77	-0,88	-0,47	0,00	0,00	0,00	-0,43	-0,86	-1,75
-1,10	-0,44	0,00	0,00	0,00	0,00	0,00	-0,42	-1,01
-0,77	0,00	0,00	0,00	0,00	0,00	0,00	0,00	-0,67
-0,67	0,00	0,00	0,00	0,00	0,00	0,00	0,00	-0,60
-0,81	0,00	0,00	0,00	0,00	0,00	0,00	0,00	-0,68
-1,16	-0,46	0,00	0,00	0,00	0,00	0,00	0,00	-0,94

-1,89	-0,89	-0,45	0,00	0,00	0,00	0,00	-0,73	-1,51
-3,05	-1,75	-1,06	-0,73	-0,64	-0,68	-0,90	-1,49	-2,52

The cylindrical power is -0.60 dpt in average, the standard deviation amounts 0.79 dpt. Neither the high aberrances of the spherical power nor the high cylinders were expected. The values increase strongly at larger angles. The measurement was repeated for the first quadrant with a switch in adjustments of the focimeter. The contact lens mode was activated to reduce the aperture pupil and therefore the high aberrances.

Table 9: Spherical power of a +6 dpt aspherical lens in contact lens mode.

11,02	8,56	7,42	6,99	6,78
8,67	7,07	6,47	6,22	6,16
7,48	6,44	6,11	6,02	5,99
7,00	6,22	6,00	5,97	5,96
6,84	6,17	5,99	5,97	5,96

The spherical power is 6.78 dpt in average, the standard deviation amounts 1.71 dpt.

Table 10: Cylindrical power of a +6 dpt aspherical lens in contact lens mode.

-3,42	-1,91	-1,18	-0,86	-0,70
-1,88	-0,87	-0,47	-0,28	-0,24
-1,12	-0,43	-0,17	-0,10	0,00
-0,80	-0,25	0,00	0,00	0,00
-0,69	-0,21	0,00	0,00	0,00

The cylindrical power is -0.62 dpt in average, the standard deviation amounts 0.81 dpt. Obviously the deviations (up to a cylinder of -3.42 dpt) increase with and increased angle. The data's quality did not improve, thus the focimeter was exchanged with the Tomey focimeter. We assume that the HLM–7000 is too sensitive for the high tilt of a test lens. The lens was measured again with the Tomey TL–3000A.

Table 11: Spherical power of a +6 dpt aspherical lens (Tomey TL–3000A).

6,33	6,32	6,23	6,23	6,19	6,21	6,28	6,31	6,40
6,27	6,18	6,18	6,10	6,08	6,03	6,13	6,22	6,38
6,20	6,09	6,01	5,94	5,94	5,97	6,01	6,12	6,21
6,14	6,05	5,96	5,93	5,91	5,91	5,98	6,10	6,22
6,16	6,05	5,94	5,92	5,92	5,92	6,00	6,11	6,23
6,20	6,10	5,98	5,94	5,93	5,97	5,97	6,06	6,28

6,25	6,17	6,06	5,99	5,98	6,06	6,05	6,12	6,35
6,35	6,28	6,19	6,13	6,10	6,14	6,14	6,22	6,41
6,37	6,37	6,29	6,25	6,25	6,29	6,28	6,35	6,45

The spherical power is 6.14 dpt in average, the standard deviation amounts 0.147 dpt.

Table 12: Cylindrical power of a +6 dpt aspherical lens (Tomey TL–3000A).

-0,36	-0,28	-0,28	-0,23	-0,24	-0,22	-0,27	-0,38	-0,52
-0,32	-0,20	-0,23	-0,11	-0,13	-0,11	-0,17	-0,33	-0,43
-0,29	-0,17	-0,10	0,00	0,00	-0,07	-0,12	-0,24	-0,37
-0,21	-0,10	0,00	0,00	0,00	0,00	-0,10	-0,21	-0,34
-0,23	-0,13	0,00	0,00	0,00	0,00	-0,10	-0,23	-0,40
-0,23	-0,14	0,00	0,00	0,00	-0,08	-0,10	-0,19	-0,45
-0,29	-0,19	-0,11	0,00	0,00	-0,13	-0,12	-0,22	-0,49
-0,43	-0,35	-0,23	-0,15	-0,11	-0,18	-0,19	-0,29	-0,56
-0,49	-0,44	-0,33	-0,27	-0,27	-0,34	-0,34	-0,44	-0,64

The cylindrical power is -0.21 dpt in average, the standard deviation amounts 0.16 dpt. The values increase for spherical and cylindrical power (for larger angles) and that was expected due to the optical aberrations astigmatism and refraction error (see chapter 2.2.2.5 Astigmatism and chapter 2.2.2.6 Image surfaces and refraction error). From now on all measurements were performed with the Tomey TL–3000A lensmeter.

3.4 Measuring

The measuring of the four lenses was performed with the measuring device attached to the Tomey TL–3000A lensmeter. The adjustments were the same as during the test measuring, the measured data were written manually into Excel-tables.

For the two lenses of +4 dpt and two lenses of -4 dpt respectively in spherical and aspherical design which results in matrix-fields of 9x9 measuring points of spherical and cylindrical power. Therefore the measuring device was rotated around its x- and y-axis (see chapter 3.2 Measuring Arrangement).

4 Measurement Results

In this chapter the results of measurement are presented using the form of matrixes. Measured and evaluated are fields of 9x9 measuring points, first the spherical and second the cylindrical powers are shown all in dpt. The matrixes are colored; the green color indicates the central value, the central value plus 0.5 dpt is orange and the central value minus 0.5 dpt is blue.

+4 dpt spherical lens

The +4 dpt spherical lens' measurement results in spherical power are presented in the subsequent table.

Table 13: Spherical power of a +4 dpt spherical lens.

4,42	4,33	4,26	4,24	4,24	4,26	4,31	4,37	4,47
4,30	4,20	4,15	4,11	4,11	4,13	4,19	4,26	4,38
4,23	4,15	4,09	4,06	4,06	4,07	4,11	4,20	4,32
4,18	4,08	3,99	3,97	3,99	4,01	4,07	4,16	4,28
4,16	4,04	4,01	4,00	4,00	4,00	4,03	4,14	4,27
4,19	4,10	4,01	3,98	3,99	4,02	4,09	4,17	4,30
4,23	4,13	4,05	4,02	4,03	4,09	4,15	4,24	4,34
4,30	4,20	4,13	4,08	4,08	4,12	4,19	4,29	4,42
4,42	4,32	4,25	4,22	4,21	4,24	4,31	4,41	4,52

The central vertex power of +4.00 dpt increases with larger angle of incidence to a maximum of 4.52 dpt. The +4 dpt spherical lens' measurement results in cylindrical power are presented in the subsequent table.

Table 14: Cylindrical power of a +4 dpt spherical lens.

-0,43	-0,35	-0,27	-0,25	-0,26	-0,29	-0,33	-0,41	-0,51
-0,29	-0,20	-0,16	-0,13	-0,12	-0,17	-0,23	-0,29	-0,40
-0,21	-0,14	-0,08	-0,08	-0,08	-0,08	-0,13	-0,19	-0,33
-0,17	-0,09	0,00	0,00	0,00	-0,10	-0,14	-0,24	-0,35
-0,15	0,00	0,00	0,00	0,00	0,00	0,00	-0,15	-0,30
-0,17	-0,09	0,00	0,00	0,00	-0,07	-0,12	-0,21	-0,34
-0,19	-0,10	0,00	0,00	0,00	-0,11	-0,18	-0,27	-0,37
-0,28	-0,20	-0,13	-0,07	-0,07	-0,13	-0,23	-0,34	-0,46
-0,42	-0,32	-0,24	-0,22	-0,19	-0,22	-0,31	-0,42	-0,56

The central cylindrical power of 0.00 dpt increases with higher angle of incidence to a maximum of -0.56 dpt.

+4 dpt aspherical lens

The +4 dpt aspherical lens' measurement results in spherical power are presented in the subsequent table.

Table 15 Spherical power of a +4 dpt aspherical lens.

3,89	3,84	3,84	3,81	3,81	3,81	3,86	3,89	3,95
3,83	3,79	3,80	3,81	3,82	3,81	3,81	3,84	3,89
3,80	3,82	3,85	3,88	3,90	3,88	3,87	3,85	3,87
3,78	3,80	3,85	3,89	3,89	3,87	3,86	3,82	3,87
3,79	3,83	3,89	3,93	3,94	3,93	3,90	3,87	3,84
3,80	3,83	3,87	3,92	3,93	3,91	3,87	3,85	3,89
3,79	3,82	3,85	3,87	3,90	3,89	3,86	3,89	3,92
3,79	3,80	3,82	3,88	3,89	3,88	3,89	3,91	3,97
3,84	3,78	3,79	3,79	3,84	3,85	3,88	3,92	4,02

The central vertex power of +3.94 dpt first decreases to a minimum of 3.79 dpt but with larger angles of incidence it increases again. The +4 dpt aspherical lens' measurement results in cylindrical power are presented in the subsequent table.

Table 16: Cylindrical power of a +4 dpt aspherical lens.

-0,16	-0,10	-0,07	0,00	0,00	0,00	-0,09	-0,14	-0,24
-0,08	0,00	0,00	0,00	0,00	0,00	0,00	-0,08	-0,16
0,00	0,00	0,00	0,00	0,00	0,00	0,00	0,00	-0,07
0,00	0,00	0,00	0,00	0,00	0,00	0,00	0,00	-0,11
0,00	0,00	0,00	0,00	0,00	0,00	0,00	0,00	0,00
0,00	0,00	0,00	0,00	0,00	0,00	0,00	0,00	-0,11
0,00	0,00	0,00	0,00	0,00	0,00	0,00	-0,09	-0,17
0,00	0,00	0,00	-0,08	-0,07	-0,07	-0,09	-0,14	-0,24
-0,10	0,00	0,00	0,00	-0,07	-0,09	-0,13	-0,21	-0,35

The central cylindrical power of 0.00 dpt increases with higher angle of incidence to a maximum of -0.35 dpt.

-4 dpt spherical lens

The -4 dpt spherical lens' measurement results in spherical power are presented in the subsequent table.

Table 17: Spherical power of a -4 dpt spherical lens.

-3,66	-3,73	-3,78	-3,80	-3,79	-3,80	-3,77	-3,74	-3,69
-3,69	-3,73	-3,83	-3,84	-3,87	-3,87	-3,85	-3,79	-3,75
-3,71	-3,77	-3,86	-3,89	-3,90	-3,91	-3,91	-3,84	-3,75
-3,72	-3,82	-3,88	-3,90	-3,90	-3,92	-3,94	-3,89	-3,76
-3,72	-3,81	-3,90	-3,91	-3,93	-3,92	-3,92	-3,88	-3,73
-3,75	-3,81	-3,86	-3,88	-3,89	-3,89	-3,90	-3,80	-3,71
-3,69	-3,77	-3,84	-3,91	-3,92	-3,92	-3,88	-3,82	-3,71
-3,64	-3,69	-3,73	-3,77	-3,77	-3,75	-3,69	-3,64	-3,64
-3,60	-3,64	-3,65	-3,66	-3,70	-3,67	-3,66	-3,64	-3,62

The central vertex power of -3.93 dpt increases with larger angle of incidence to a maximum of -3.60 dpt. The -4 dpt spherical lens' measurement results in cylindrical power are presented in the subsequent table.

Table 18: Cylindrical power of a -4 dpt spherical lens.

-0,07	-0,07	0,00	0,00	0,00	0,00	0,00	0,00	0,00
-0,10	-0,09	0,00	0,00	0,00	0,00	0,00	0,00	0,00
-0,08	-0,08	0,00	0,00	0,00	0,00	0,00	0,00	0,00
-0,08	0,00	0,00	0,00	0,00	0,00	0,00	0,00	-0,09
-0,12	0,00	0,00	0,00	0,00	0,00	0,00	0,00	-0,08
0,00	0,00	0,00	0,00	0,00	0,00	0,00	0,00	-0,12
-0,17	-0,14	-0,09	0,00	0,00	0,00	0,00	0,00	-0,08
-0,12	-0,11	-0,10	-0,09	-0,11	-0,14	-0,16	-0,17	-0,14
-0,15	-0,15	-0,18	-0,15	-0,15	-0,15	-0,14	-0,12	-0,13

The central cylindrical power of 0.00 dpt increases with higher angle of incidence to a maximum of -0.15 dpt.

-4 dpt aspherical lens

The -4 dpt aspherical lens' measurement results in spherical power are presented in the subsequent table.

Table 19: Spherical power of a -4 dpt aspherical lens.

-3,93	-3,97	-3,98	-3,98	-3,98	-3,98	-3,98	-3,97	-3,96
-3,95	-3,97	-3,99	-3,97	-3,97	-3,98	-3,99	-3,99	-4,00
-3,95	-3,97	-3,98	-3,96	-3,97	-3,98	-3,99	-3,99	-3,98
-3,97	-4,01	-3,98	-3,96	-3,97	-4,00	-3,98	-3,99	-3,99
-3,98	-4,00	-3,97	-3,97	-3,98	-4,00	-4,02	-3,99	-3,98
-3,93	-3,92	-3,94	-3,92	-3,94	-3,93	-3,95	-3,94	-3,95
-4,02	-4,03	-4,00	-3,99	-4,00	-4,01	-3,99	-4,00	-4,00
-3,96	-3,99	-3,98	-3,98	-3,98	-4,00	-3,96	-3,96	-3,95
-3,98	-4,01	-4,01	-3,98	-3,97	-3,98	-3,97	-3,97	-3,94

The central vertex power of -3.98 dpt is almost constant for the whole lens. The -4 dpt aspherical lens' measurement results in cylindrical power are presented in the subsequent table.

Table 20: Cylindrical power of a -4 dpt aspherical lens.

-0,17	-0,16	-0,18	-0,17	-0,20	-0,20	-0,24	-0,26	-0,29
-0,16	-0,16	-0,14	-0,14	-0,14	-0,16	-0,16	-0,19	-0,23
-0,15	-0,13	-0,09	-0,08	-0,08	-0,08	-0,11	-0,14	-0,22
-0,09	0,00	0,00	0,00	0,00	0,00	-0,09	-0,14	-0,18
-0,07	0,00	0,00	0,00	0,00	0,00	0,00	-0,11	-0,17
-0,11	-0,10	0,00	0,00	0,00	-0,07	-0,11	-0,16	-0,22
0,00	0,00	0,00	0,00	0,00	0,00	-0,09	-0,14	-0,21
-0,07	0,00	0,00	0,00	0,00	0,00	-0,12	-0,18	-0,26
0,00	0,00	0,00	-0,08	-0,10	-0,12	-0,18	-0,24	-0,28

The central cylindrical power of 0.00 dpt increases with higher angle of incidence to a maximum of -0.29 dpt.

5 Analysis

The refractive error and the astigmatism (see chapters 2.2.2.5 Astigmatism and 2.2.2.6 Image surfaces and refraction error) are supposed to have the major impact on the measurement results. Thus the measurement values are analyzed in respect to both errors.

For a better comparability the values of all measuring points of each lens which have the same distance to the center (optical axis) were averaged. This is possible because single vision ophthalmic lenses are generally axially symmetric. The approach is illustrated in the subsequent table 21, the values with the same distance to the center are marked with the same letter and the same color. For example “E” is the result of an average of four values and “I” is the result of an average of eight values. Therefore the bold-rimmed quadrant covers all measurement results and in the following chapters only this quadrant is presented.

Table 21: Measuring points with the same distance to the lens’ center are marked with color and letters.

F	G	H	I	E	I	H	G	F
G	K	L	M	D	M	L	K	G
H	L	N	O	C	O	N	L	H
I	M	O	P	B	P	O	M	I
E	D	C	B	A	B	C	D	E
I	M	O	P	B	P	O	M	I
H	L	N	O	C	O	N	L	H
G	K	L	M	D	M	L	K	G
F	G	H	I	E	I	H	G	F

To validate the measured values, these are compared to a calculation. This is shown in the next chapter.

5.1 Calculation

The tangential and sagittal oblique vertex sphere powers of the +4 dpt spherical lens are calculated manually in this chapter. The object distance a_1=t_1 is chosen -1000000 mm and the height of incidence U_2' is 20°. The front vertex power $F_{measured}$ is measured with a spherometer designed for a refractive index of 1.525. Using equation 6 one can calculate the front vertex power F_1 for a differing refractive index n.

$$F_1 = F_{measured}\ \frac{n-1}{0{,}525} \qquad \text{EQ 6}$$

The thickness of the lens d with a thickness gauge and the width $l = 2r_b$ of the lens is measured with a PD scale. Radius of rotation $r_{rotation}$ and the offset z are given by the geometry of the technical device. Table 22 gives an overview of the given values.

Table 22: Given values for the calculation of the tangential and sagittal oblique vertex powers of a +4 dpt spherical lens.

$F_{measured}$/ F_1	6.0 dpt/ 6.9 dpt
S'	4.0 dpt
n	1.6
d	4.7 mm
l	58 mm
$r_{rotation}$	28.5 mm
z	1.5 mm
U_2'	$20° = \frac{\pi}{9}$
$a_1 = t_1$	$-1\text{km} = -1\text{‘}000\text{‘}000$ mm

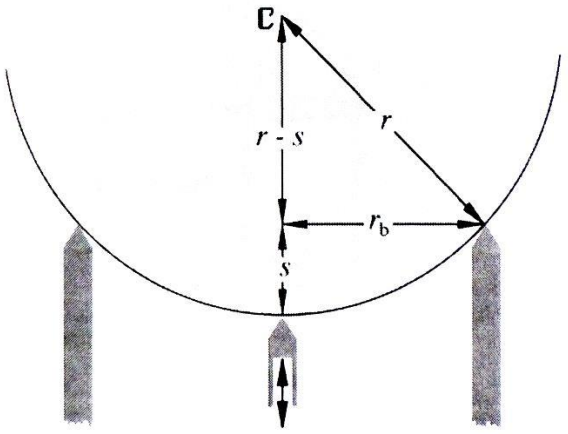

Fig. 21:The principle of the spherometer (Smith, Atchison 1997).

$$r^2 = {r_b}^2 + (r - s)^2 \qquad \textbf{EQ 7}$$

$$\rightarrow \quad s = r_2 - \sqrt{r_2^2 - \left(\frac{l}{2}\right)^2} \qquad \textbf{EQ 8}$$

$$s = 197.2\ mm - \sqrt{\left(197.2\ mm\right)^2 - \left(\frac{58\ mm}{2}\right)^2} = 2{,}1\ mm$$

$$b' = r_{rotation} - z + s \qquad \textbf{EQ 9}$$

$$b' = 28.5\ mm - 1.5\ mm + 2.1\ mm = 29.1\ mm$$

$$F_1 = F_{measured}\ \frac{n-1}{0.525} \qquad \textbf{EQ 10}$$

$$F_1 = 6.0\ dpt\ \frac{1.6-1}{0.525} = 6.9\ dpt$$

5.1.1 Meridional calculation against direction of the light

a) Fraction at second surface

$$\sin I_2' = \frac{b'-r_2}{r_2} \sin U_2' \qquad \textbf{EQ 11}$$

$$S' = \frac{F_1}{1-\frac{d}{n}F_1} + F_2 \qquad \textbf{EQ 12}$$

$$\rightarrow F_2 = S' - \frac{F_1}{1-\frac{d}{n}F_1} \qquad \textbf{EQ 13}$$

$$F_2 = 4.0dpt - \frac{6.9\ dpt}{1-\frac{4.7\ mm}{1.6}\ 6.9\ dpt} = -3.0\ dpt$$

$$r = \frac{n_0-1}{F} \qquad \textbf{EQ 14}$$

$$\rightarrow r_2 = \frac{1-n}{F_2} \qquad \textbf{EQ 15}$$

$$r_2 = \frac{1-1.6}{-3.0\ dpt} = 197.2\ mm$$

$$\sin I_2' = \frac{29.1\ mm - 197.2\ mm}{197.2\ mm}\ 0.3 = -0.3$$

$$\sin I_2 = \frac{\sin I_2'}{n} \qquad \text{EQ 16}$$

$$\sin I_2 = \frac{-0.3}{1.6} = -0.2$$

$$U_2 = U_2' + I_2' - I_2 \qquad \text{EQ 17}$$

$$U_2 = \frac{\pi}{9} + \arcsin(-0{,}3) - \arcsin(-0{,}2) = 0{,}2$$

$$s_2 = r_2\left(1 + \frac{\sin I_2}{\sin U_2}\right) \qquad \text{EQ 18}$$

$$s_2 = 197.2\ mm\left(1 + \frac{-0{,}2}{\sin 0{,}2}\right) = 43.9\ mm$$

b) Transfer to surface one

$$s_1' = s_2 + d \qquad \text{EQ 19}$$

$$s_1 = 43.9\ mm + 4.7\ mm = 48.6\ mm$$

$$U_1' = U_2 = 0.2 \qquad \text{EQ 20}$$

c) Fraction at surface one

$$r = \frac{n_0 - 1}{F} \qquad \text{EQ 21}$$

$$\rightarrow r_1 = \frac{n-1}{F_1} \qquad \text{EQ 22}$$

$$r_1 = \frac{1.6-1}{6.9\ dpt} = 87.0\ mm$$

$$\sin I_1' = \left(\frac{s_1}{r_1} - 1\right)\sin U_1' \qquad \text{EQ 23}$$

$$\sin I_1' = \left(\frac{48.6\ mm}{87.0\ mm} - 1\right)\sin 0.2 = -0.1$$

$$\sin I_1 = n\ \sin I_1' \qquad \text{EQ 24}$$

$$\sin I_1 = 1.6\sin(-0.1) = -0.2$$

$$U_1 = U_1' + I_1' - I_1 \qquad \text{EQ 25}$$

$$U_1 = 0.2 + \arcsin(-0.1) - \arcsin(-0.2) = 0.3$$

5.1.2 Paraxial optic following the principle ray

Astigmatic surface power F^{ast}:

$$F^{ast} = \frac{n\cos I_1' - \cos I_1}{r_1} \qquad \text{EQ 26}$$

Coddington equations:

Tangential: $t = s_t \quad \rightarrow \quad \frac{n'}{t'}\cos^2 I' - \frac{n}{t}\cos^2 I = F^{ast}$ EQ 27

Sagittal: $a = s_s \rightarrow \frac{n'}{t'} - \frac{n}{t} = F^{ast}$ **EQ 28**

a) Fractiton at surface one:

$F_1^{ast} = \frac{n \cos I_1' - \cos I_1}{r_1}$ **EQ 29**

$F_1^{ast} = \frac{1.6 \cos(-0.1) - \cos(-0.2)}{87.0\ mm} = 0.007$

Tangential:

$t_1' = \frac{n\ \cos^2 I_1'}{F_1^{ast} + \frac{\cos^2 I_1}{t_1}}$ **EQ 30**

$t_1' = \frac{1.6\ \cos^2(-0.1)}{0.007 + \frac{\cos^2(-0.2)}{-1\ km}} = 227{,}5\ mm$

Sagittal:

$a_1' = \frac{n}{F_1^{ast} + \frac{1}{a_1}}$ **EQ 31**

$a_1' = \frac{1.6}{0.007 + \frac{1}{-1\ km}} = 230.0\ mm$

b) Transfer to surface two (all angles I and U are inserted negative):

$\varphi_1 = I_1 - U_1$ **EQ 32**

$\varphi_1 = -0.2 + 0.3 = 0.13$

$\varphi_2 = I_2' - U_2'$ **EQ 33**

$\varphi_2 = -0.3 + \frac{\pi}{9} = 0.05$

$p_1 = r_1\ (1 - \cos \varphi_1)$ **EQ 34**

$p_1 = 87.0\ mm\ (1 - \cos 0.13) = 0.8\ mm$

$p_2 = r_2\ (1 - \cos \varphi_2)$ **EQ 35**

$p_2 = 197.2\ mm\ (1 - \cos 0.05) = 0.3\ mm$

Oblique gauge:

$\tilde{d} = \frac{d + p_2 + p_1}{\cos U_2}$ **EQ 36**

$\tilde{d} = \frac{4.7\ mm + 0.3\ mm + 0.8\ mm}{\cos 0.2} = 4.3\ mm$

c) Fraction at surface two:

$F_2^{ast} = \frac{\cos I_2' - n\ \cos I_2}{r_2}$ **EQ 37**

$F_2^{ast} = \frac{\cos(-0.3) - 1.6 \cos(-0.2)}{197.2\ mm} = -0.003$

Tangential:

$$t_2 = t_1' - \tilde{d} \qquad \textbf{EQ 38}$$

$$t_2 = 227.5\,mm - 4.3\,mm = 223.1\,mm$$

$$t_2' = \frac{\cos^2 I_2'}{F_2^{ast} + \frac{\mathrm{n}\cos^2 I_2}{t_2}} \qquad \textbf{EQ 39}$$

$$t_2' = \frac{\cos^2(-0.3\,mm)}{-0.003 + \frac{1.6\cos^2(-0.2)}{223.1\,mm}} = 240.4\,mm$$

Sagittal:

$$a_2 = a_1' - \tilde{d} \qquad \textbf{EQ 40}$$

$$a_2 = 230.0\,mm - 4.3\,mm = 225.6\,mm$$

$$a_2' = \frac{1}{F_2^{ast} + \frac{n}{a_2}} \qquad \textbf{EQ 41}$$

$$a_2' = \frac{1}{-0.003 + \frac{1.6}{225.6\,mm}} = 252.2\,mm$$

d) Focal distances‘ reference to the vertex sphere:

$$\delta_{s'} = -\frac{r_2 \sin\varphi_2}{\sin U_2'} - b' \qquad \textbf{EQ 42}$$

$$\delta_{s'} = -\frac{197.2\,mm \sin 0.05}{\sin\frac{\pi}{9}} = 1.6\,mm$$

$$T_{VS}' = (t_2' - \delta_{s'})^{-1} \qquad \textbf{EQ 43}$$

$$T_{VS}' = (240.4\,mm - 1.6\,mm)^2 = 4.19\,dpt$$

$$A_{VS}' = (a_2' - \delta_{s'})^{-1} \qquad \textbf{EQ 44}$$

$$A_{VS}' = \left(252.2\,mm - 1.6\,mm\right)^{-1} = 3.99\,dpt$$

The tangential power is 4.19 dpt, the sagittal power is 3.99 dpt. Following this schema it is possible to create a program in Excel, which calculates the tangential and sagittal powers for several heights of incidence. Such a program was written by Prof. Dr. Baumbach of Aalen University. The program’s result for the +4 dpt spherical lens at 20° equal the manual calculation, so it was used to validate all measured results.

Table 23: Computation of the tangential and sagittal oblique vertex sphere powers of the +4 dpt spherical lens with an object distance of 1’000’000 mm.

Angle of incidence	0°	5°	10°	15°	20°
Tangential [dpt]	4,00	4,01	4,05	4,11	4,19
Sagittal [dpt]	4,00	4,00	4,00	4,00	3,99

The program in Excel calculates the tangential and sagittal oblique vertex sphere powers of a lens in 5°-steps, but only on the x- and y-axis.

5.2 Comparison of averaged measuring results and calculated oblique astigmatism

The measured data of the two lenses of spherical design is compared to the computed results by Pearson's correlation coefficient r. This coefficient is a measure of the correlation of two variables X and Y, giving a value between ±1. A value of 1 is total positive correlation, -1 is total negative and 0 is no correlation. The coefficient r is given by the following equation.

$$r = \frac{\sum(x_i - \bar{x})(y_i - \bar{y})}{\sqrt{\sum(x_i - \bar{x})^2}\sqrt{\sum(y_i - \bar{y})^2}} \qquad \text{EQ 45}$$

Anymore spherical and cylindrical powers are set in relation separately at each measuring point on the x- and y-axis.

+4 dpt spherical lens

The averaged values of measured data for the +4 dpt spherical lens' spherical power are presented in the subsequent table.

Table 24: Averaged spherical power of a +4 dpt spherical lens.

4,22	4,24	4,31	4,37	4,46
4,09	4,12	4,17	4,24	4,37
4,03	4,05	4,10	4,17	4,31
4,00	4,00	4,05	4,12	4,24
4,00	4,00	4,03	4,09	4,22

For the computation of sagittal and tangential oblique sphere powers see the antecedent chapter 5.1, calculation. Table 25 gives an overview of the given values.

Table 25: Given values for the calculation of the tangential and sagittal oblique vertex powers of a +4 dpt spherical lens.

$F_{measured}$/ F_1	6.0 dpt/ 6.9 dpt
S'	4.0 dpt
n	1.6
d	4.7 mm
l	58 mm
$r_{rotation}$	28.5 mm
z	1.5 mm
U_2'	$20° = \frac{\pi}{9}$
$a_1 = t_1$	$-1\text{km} = -1‘000‘000$ mm

The computed spherical power of the +4 dpt spherical lens for angles of 0°, 5°, 10°, 15°, and 20° is presented below.

Table 26: Computed spherical power of a +4 dpt spherical lens for angles of 0° (left), 5°, 10°, 15°, and 20°.

4,00	4,01	4,05	4,11	4,19

The difference of measured and computed spherical power is to identify errors within the measured data. The value of potential differences shows the gravity of these errors.

Table 27: Difference of measured and computed spherical power of a +4 dpt spherical lens for angles of 0° (left), 5°, 10°, 15°, and 20°.

0,01	-0,01	-0,01	-0,01	0,03

The difference of measured and computed spherical power is 0.00 dpt in average, the standard deviation amounts 0.02 dpt. Minimum is -0.01 dpt and Maximum is 0.03 dpt. The measured results and the computed data correlate on a level of 0,99.

The averaged values of measured data for the +4 dpt spherical lens’ cylindrical power are presented in the subsequent table.

Table 28: Averaged cylindrical power of a +4 dpt spherical lens.

-0,23	-0,25	-0,31	-0,38	-0,48
-0,09	-0,14	-0,18	-0,26	-0,38
-0,02	-0,07	-0,10	-0,18	-0,31
0,00	-0,04	-0,07	-0,14	-0,25
0,00	0,00	-0,02	-0,09	-0,23

The computed cylindrical power is presented in table 29.

Table 29: Computed cylindrical power of a +4 dpt spherical lens for angles of 0° (left), 5°, 10°, 15°, and 20°.

0,00	-0,01	-0,05	-0,11	-0,20

The difference of measured and computed cylindrical power for the +4 dpt spherical lens is presented in the subsequent table.

Table 30: Difference of measured and computed cylindrical power of a +4 dpt spherical lens for angles of 0° (left), 5°, 10°, 15°, and 20°.

0,00	0,01	0,03	0,02	-0,03

The difference of measured and computed cylindrical power is 0.02 dpt in average, the standard deviation amounts 0.02 dpt. The minimum is -0.03 dpt and the maximum is 0.03 dpt. The measured results and the computed data are in good agreement (0,98). The tangential and sagittal refractive powers are illustrated in the subsequent figure.

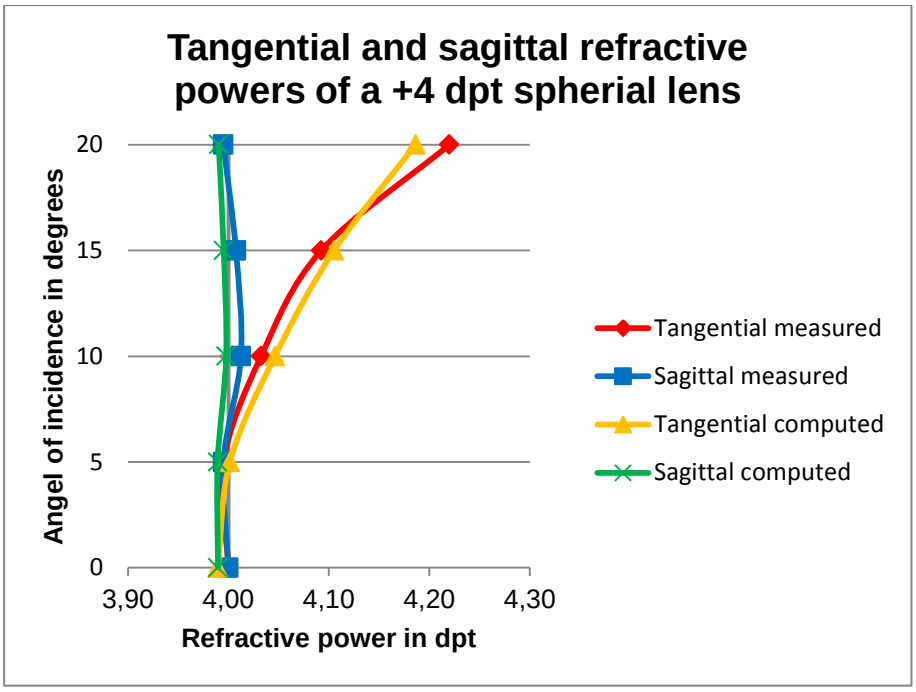

Fig. 22: The graph shows the correlation of calculated and measured sagittal and tangential powers of a +4 dpt spherical lens.

The sagittal powers are quite consistent on a level of +4,00 dpt starting at 0° until the end of the measuring range (20°). The sagittal powers also start at +4.00 dpt at the center but with increasing angle of the viewing direction the sagittal power increases, too. The computed values and the measured ones are in good agreement.

-4 dpt spherical lens

The averaged values of measured data for the -4 dpt spherical lens' spherical power are presented in the subsequent table.

Table 31: Averaged Spherical power of a -4 dpt spherical lens.

-3,74	-3,73	-3,70	-3,68	-3,64
-3,83	-3,82	-3,79	-3,71	-3,68
-3,91	-3,90	-3,87	-3,79	-3,70
-3,91	-3,90	-3,90	-3,82	-3,73
-3,93	-3,91	-3,91	-3,83	-3,74

For computation of sagittal and tangential oblique sphere powers the following values were given.

Table 32: Given values for the calculation of the tangential and sagittal oblique vertex powers of a -4 dpt spherical lens.

$F_{measured}/ F_1$	4.25 dpt/ 4.25 dpt
S'	$-3{,}93$ dpt
n	1.525
d	1,2 mm
l	54 mm
$r_{rotation}$	28.5 mm
z	1.5 mm
U_2'	$20° = \frac{\pi}{9}$
$a_1 = t_1$	$-1\text{km} = -1‘000‘000$ mm

The computed spherical power of the -4 dpt spherical lens for angles of 0°, 5°, 10°, 15°, and 20° is presented below.

Table 33: Computed spherical power of a -4 dpt spherical lens for angles of 0° (left), 5°, 10°, 15°, and 20°.

-3,93	-3,93	-3,91	-3,88	-3,83

The difference of measured and computed spherical power for the -4 dpt spherical lens is presented in the subsequent table.

Table 34: Difference of measured and computed spherical power of a -4 dpt spherical lens for angles of 0° (left), 5°, 10°, 15°, and 20°.

0,00	0,02	0,00	0,04	0,09

The difference of measured and computed spherical power is 0.04 dpt in average, the standard deviation amounts 0.04 dpt. The minimum is 0.00 dpt and the maximum is 0.09 dpt. The measured results and the computed data coincide quite good at 0,98.

The averaged values of measured data for the -4 dpt spherical lens' cylindrical power are presented in the subsequent table.

Table 35: Averaged cylindrical power of a -4 dpt spherical lens.

-0,09	-0,07	-0,08	-0,09	-0,09

-0,03	-0,03	-0,06	-0,09	-0,09
0,00	0,00	-0,02	-0,06	-0,08
0,00	0,00	0,00	-0,03	-0,07
0,00	0,00	0,00	-0,03	-0,09

The computed cylindrical power is presented below.

Table 36: Computed cylindrical power of a -4 dpt spherical lens for angles of 0° (left), 5°, 10°, 15°, and 20°.

0,00	0,00	0,00	-0,01	-0,03

The difference of measured and computed cylindrical power for the -4 dpt spherical lens is presented in the subsequent table.

Table 37: Difference of measured and computed cylindrical power of a -4 dpt spherical lens for angles of 0° (left), 5°, 10°, 15°, and 20°.

0,00	0,00	0,00	-0,02	-0,06

The difference of measured and computed cylindrical power is -0.02 dpt in average, the standard deviation amounts 0.03 dpt. Minimum is -0.06 dpt and Maximum is 0.00 dpt. The measured results and the computed data correlate on a level of 0,99. The tangential and sagittal refractive powers are illustrated in the subsequent figure.

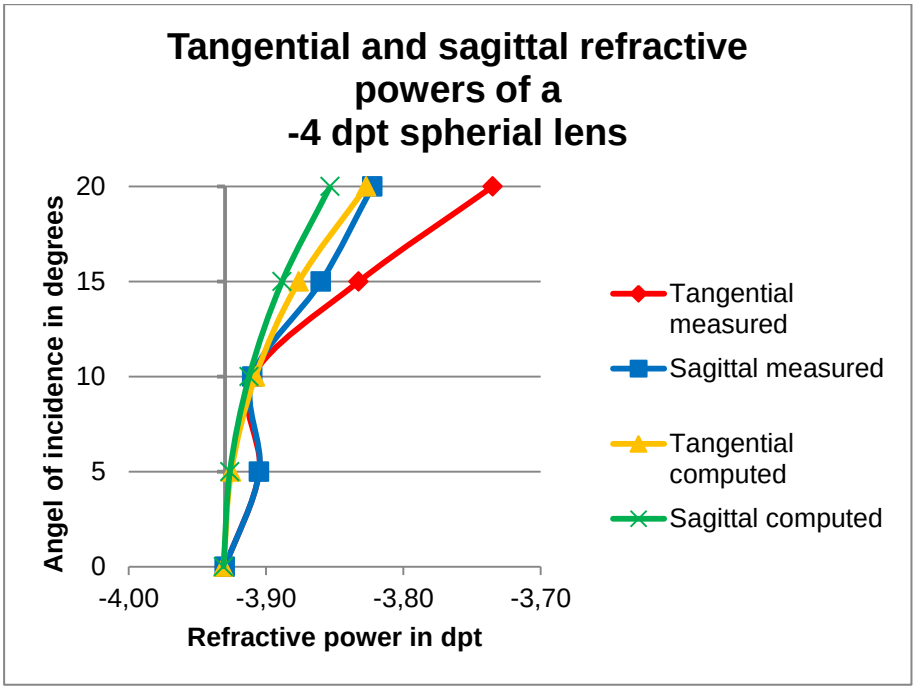

Fig. 23: The graph shows the correlation of calculated and measured sagittal and tangential powers of a -4 dpt spherical lens.

Starting at -3.93 dpt at the center of the lens the values of measured and computed powers all increase in positive direction. For both, the tangential oblique sphere

power increases slightly more. The comparison of the -4 dpt lens shows lower accordance of measurements and calculations than the comparison of the +4 dpt lens.

5.3 Comparison of spherical and aspherical lenses

Aspherical design of a lens is characterized by the surface asphericity g. The profile of an aspheric surface is more complex with the aim to reduce optical aberrations which occur from a simple lens. Those are thinner and flatter lenses without decreasing the optical performance. There is no easy possibility to calculate the expected astigmatism caused by a given angle of the viewing direction for an aspherical lens. (Smith, Atchison 1997; Nolting, Wassmer 2001) In this chapter the sagittal and tangential oblique sphere powers are compared for the aspherical and spherical designed lenses of the same vertex power.

+4 dpt aspherical lens

The results of averaging the measured data (cylindrical and spherical powers) for the +4 dpt aspherical lens are presented in the next two tables.

Table 38: Averaged spherical power of a +4 dpt aspherical lens. For the comparison the bold-rimmed data is extracted.

3,82	3,83	3,85	3,87	3,93
3,85	3,84	3,84	3,84	3,87
3,90	3,87	3,86	3,84	3,85
3,92	3,90	3,87	3,84	3,83
3,94	3,92	3,90	3,85	3,82

Table 39: Averaged cylindrical power of a +4 dpt aspherical lens.

-0,02	-0,04	-0,09	-0,13	-0,21
-0,02	-0,02	-0,02	-0,06	-0,13
0,00	0,00	0,00	-0,02	-0,09
0,00	0,00	0,00	-0,02	-0,04
0,00	0,00	0,00	-0,02	-0,02

The tangential and sagittal refractive powers for the spherical and aspherical lens of +4 dpt are illustrated in the subsequent two figures. The values of the spherical lens are gathered from the antecedent chapter; they are all reduced by 0,06 dpt to equal the central vertex power. Figure 24 illustrates the values with an x-shift of 0° and with an angle of incidence from 0° to 20° (see table 38).

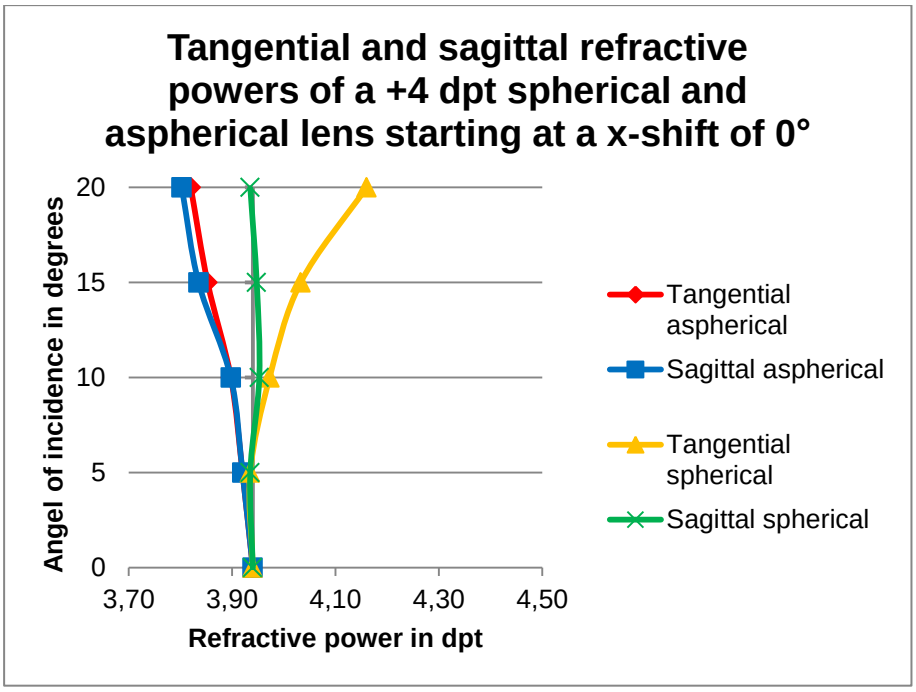

Fig. 24: Tangential and sagittal refractive powers of a +4 dpt spherical and aspherical lens starting at a x-shift of 0°.

The sagittal and tangential refractive powers of the aspherical lens decrease slightly but differ only marginal. In contrast, the sagittal power of the spherical lens stays constant at +4 dpt whereas the tangential power increases. There is a change in measuring values cognoscible when shifting the examined data 20° on the x-axis. Therefore the measuring points are further off-center.

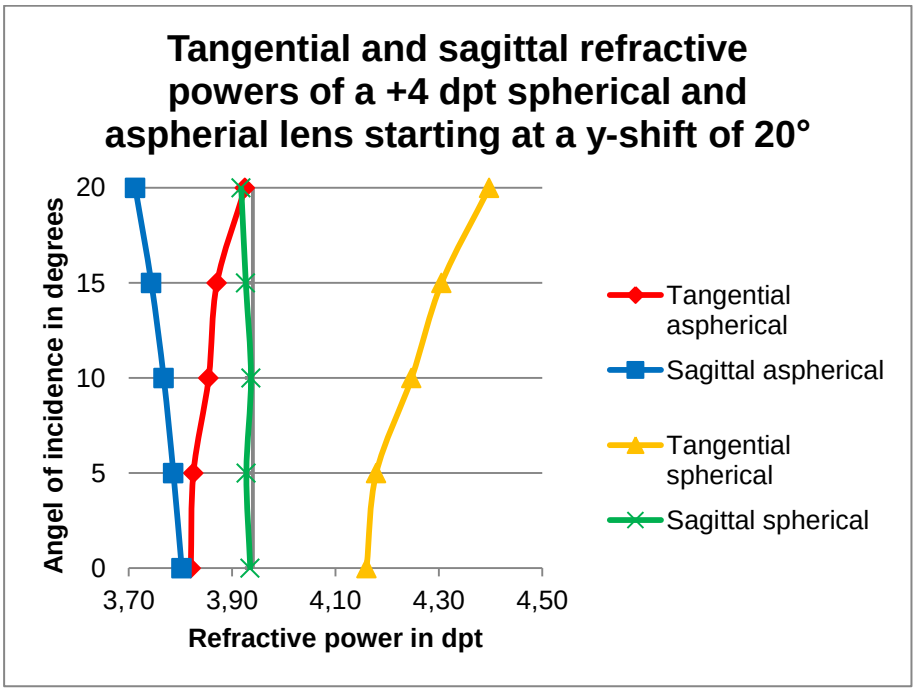

Fig. 25: Tangential and sagittal refractive powers of a +4 dpt spherical and aspherical lens starting at a x-shift of 20°.

The tangential power of the aspherical lens increases towards the central value of +4 dpt whereas the sagittal power decreases. This leads to a higher astigmatism than at the very y-axis but the combination of both is still closer to the vertex power of +4 dpt than the spherical design. There the tangential power keeps on increasing and the sagittal values stay about +4 dpt. That leads to an increasing astigmatism.

-4 dpt aspherical lens

The averaged measured data (cylindrical and spherical powers) for the -4 dpt aspherical lens is presented in the subsequent two tables.

Table 40: Averaged spherical power of a -4 dpt aspherical lens.

-3,98	-3,97	-3,98	-3,97	-3,95
-3,99	-3,97	-3,99	-3,98	-3,97
-3,99	-3,97	-3,99	-3,99	-3,98
-3,97	-3,95	-3,97	-3,97	-3,97
-3,98	-3,97	-3,99	-3,99	-3,98

Table 41: Averaged cylindrical power of a -4 dpt aspherical lens.

-0,14	-0,15	-0,15	-0,17	-0,19
-0,06	-0,09	-0,10	-0,13	-0,17
-0,02	-0,05	-0,07	-0,10	-0,15
0,00	-0,02	-0,05	-0,09	-0,15
0,00	0,00	-0,02	-0,06	-0,14

The tangential and sagittal refractive powers for the spherical and aspherical lens of -4 dpt are illustrated in the subsequent two figures. The values of the spherical lens are gathered from the antecedent chapter; they are all reduced by 0,05 dpt to equal the central vertex power. Figure 26 illustrates the values with an x-shift of 0° with an angle of incidence from 0° to 20° (see table 38).

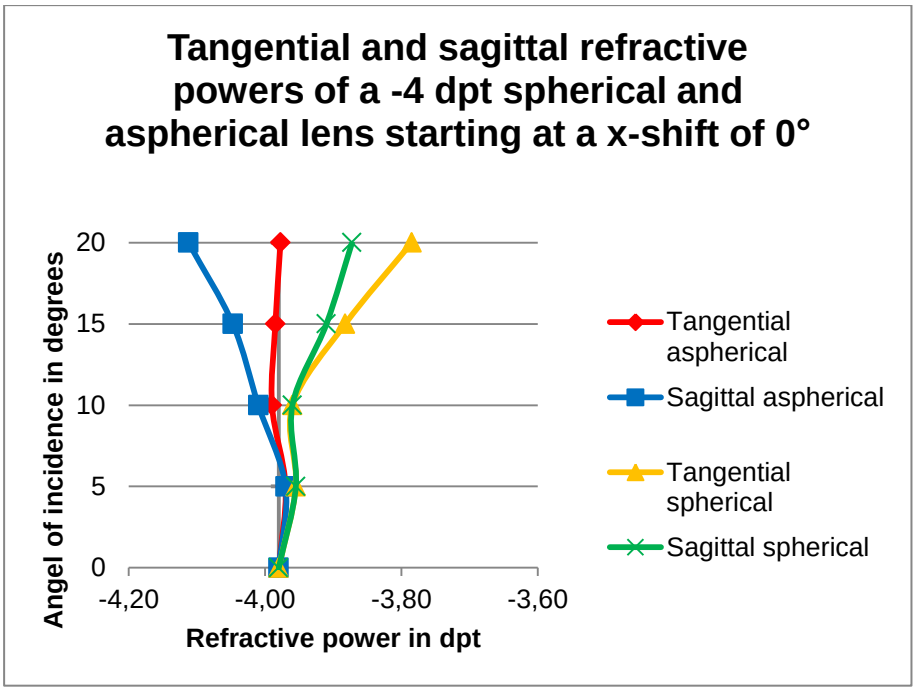

Fig. 26: Tangential and sagittal refractive powers of a -4 dpt spherical and aspherical lens starting at a x-shift of 0°.

The sagittal oblique power vertex of the aspherical lens is smaller than the vertex power of -3.98 dpt, the tangential is close to it, the values of the spherical lens both are larger than the vertex power. Both lenses' sagittal power is lower than the tangential power, far off the center the difference increases (which equals the astigmatism).

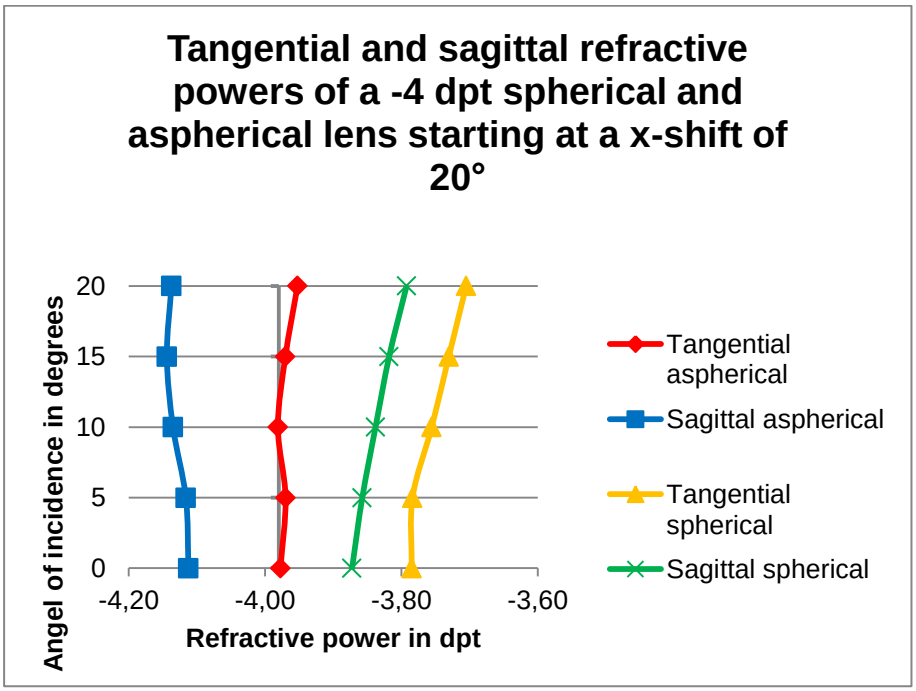

Fig. 27: Tangential and sagittal refractive powers of a -4 dpt spherical and aspherical lens starting at a x-shift of 20°.

A 20°-shift on the x-axis leads to different measuring results. The difference of oblique sagittal and tangential power and therefore the astigmatism for both lenses increases. The aspherical powers keep the central vertex power of -4 dpt in-between. In comparison the sagittal and tangential vertex powers of the aspherical and spherical lens appear to be pretty similar to each other but reflected on a point about the center.

5.4 Results

The results are concentrated and evaluated in this chapter. In the first part, the lenses of spherical design are considered and in the second part the lenses of aspherical design are discussed.

a) ±4 dpt lenses of spherical design

On average, the measuring results and the computed data of cylindrical and spherical power of the spherical designed lenses coincide at 0,98, they deviate on average by 0.01 dpt and the standard deviation amounts 0.03 dpt on average. The minimum is -0.06 dpt and the maximum is 0.09 dpt. Normal focimeters have a measuring inaccuracy of up to 0.06 dpt (Diepes, Blendowske 2002), only one measuring point is above or below this value. Therefore the quality of the measured data is very high.

b) ±4 dpt lenses of aspherical design

As explained in chapter 5.3, Comparison of spherical and aspherical lenses, it was not possible to compute data for the aspheric lenses because of the differing surface asphericity. There is no quantitative conclusion but the aspherical designed lenses were compared to the spherical ones. The impact of an aspherical design can be seen from the positive lenses than from the negative lenses. An increasing radius of the front surface towards the edges leads to less optical aberrations in those areas. Therefore an aspherical lens appears to have less astigmatism towards the edges than has a spherical lens. This effect is more distinctive for positive lenses than for negative lenses.

6 Discussion

After finishing the measurement and evaluation of the results there is the question concerning possible malfunctions. The evaluation shows that the measurement results, measuring performed with the measuring device, correlate on a very high level with the expected (proven by calculations) values. Hence one can say that the measuring device works and it is possible to measure the optical power of an ophthalmic lens due to the principle of the center of rotation of the eye.

Comparing the device to already existing measurement methods to measure a lens in accordance to principle of the center of rotation of the eye, the device is very easy to handle. One does not need a large test setup but can easily measure a lens.

The positive lens' measurement results and the calculated values differ less, than do the results of the negative lens. But as described in chapter 5.2, Comparison of averaged measuring results and calculated oblique astigmatism, they still correlate on a very high level.

Another point is the (more or less) slightly unsymmetrical distribution of the optical power which increased distance to the center. If possible scattering light comes through the windows and has interfered with the experiments. But by averaging the results the symmetry was simulated.

The tested lenses were randomly chosen and they have different refractive indexes. The measurement results would even be better comparable with lenses of the same refractive index. For the calculations the different refractive indexes were taken into account, also the different geometries and therefore different values of b'.

The measuring device was mounted on the Tomey focimeter with adhesive pads. This is not an ideal solution, but for the measurements the device was centered and adjusted as exact as possible but small disposals cannot be excluded completely.

7 Conclusion

After giving consideration to all results and the discussion, the measuring device meets the requirements very good. The possibility is given to measure a lens as in its operating situation, which is described by the principle of the center of rotation of the eye, in an easy way.

Prismatic power of the lenses was not recorded at all because the two lenses of spectacle glasses should balance each other. However a further examination would be interesting. The test lenses' sample size was pretty small, a higher number of lenses would lead to more exact results. When measuring a higher number of lenses even with more characteristics, the manual data acquisition would take too much time and would be too complicated. The Tomey TL–3000A features a RS-232C-interface; hence it is possible to send the measured data to a computer. For a further consideration of this topic it would be of benefit to write a program (e.g. with Labview, National Instruments) for the information transfer.

List of figures

List of tables

List of equations

Publication bibliography

- Chauhan, Ashok K.; Varma, A. (2009): A textbook of molecular biotechnology. New Delhi: I.K. International Pub. House.
- Diepes, Heinz; Blendowske, Ralf (2002): Optik und Technik der Brille. Mit 40 Tabellen. Heidelberg: Optische Fachveröff.
- Hecht, Eugene (2002): Optics. 4th ed. Reading, Mass: Addison-Wesley.
- Hecht, Eugene (2009): Optik. 5., verb. Aufl. München: Oldenbourg.
- Marchesi, Jost J. (2011): Photokollegium. 11., vollst. neu überarb. und erw. Aufl. Gilching: Verl. Photographie.
- Nolting, Jürgen; Wassmer, Karin (2001): Abbildungsfehler. Eine Beratungsfibel für den Augenoptiker. [Heidelberg]: Optische Fachveröff., Verl. der Dt. Optikerzeitung (Inform, H. 13).
- Smith, George; Atchison, David A. (1997): The eye and visual optical instruments. Cambridge, U.K, New York, NY, USA: Cambridge University Press.
- Wikipedia (Ed.) (2014): Shack–Hartmann wavefront sensor - Wikipedia, the free encyclopedia. Available online at

http://en.wikipedia.org/w/index.php?oldid=591887311, updated on 5/21/2014, checked on 6/9/2014.

- Zeiss, Carl (Hrsg.) (2000): Handbuch für Augenoptik. 4th ed. Oberkochen: C. Maurer.